NAVAL SHIP RESEARCH AND DEVELOPMENT CENTER

Bethesda, Maryland 20034

LAMINAR FLOW CIRCULATION IN A ROTATING TANK WITH A SPINNING COVER

Hans J. Lugt, Henry J. Haussling, Samuel Ohring

COMPUTATION AND MATHEMATICS DEPARTMENT

February 1972

Report 3797

LAMINAR FLOW CIRCULATION IN A ROTATING TANK WITH A SPINNING COVER

The Naval Ship Research and Development Center is a U. S. Navy center for laboratory effort directed at achieving improved sea and air vehicles. It was formed in March 1967 by merging the David Taylor Model Basin at Carderock, Maryland with the Marine Engineering Laboratory at Annapolis, Maryland.

Naval Ship Research and Development Center

Bethesda, Md. 20034

MAJOR NSRDC ORGANIZATIONAL COMPONENTS

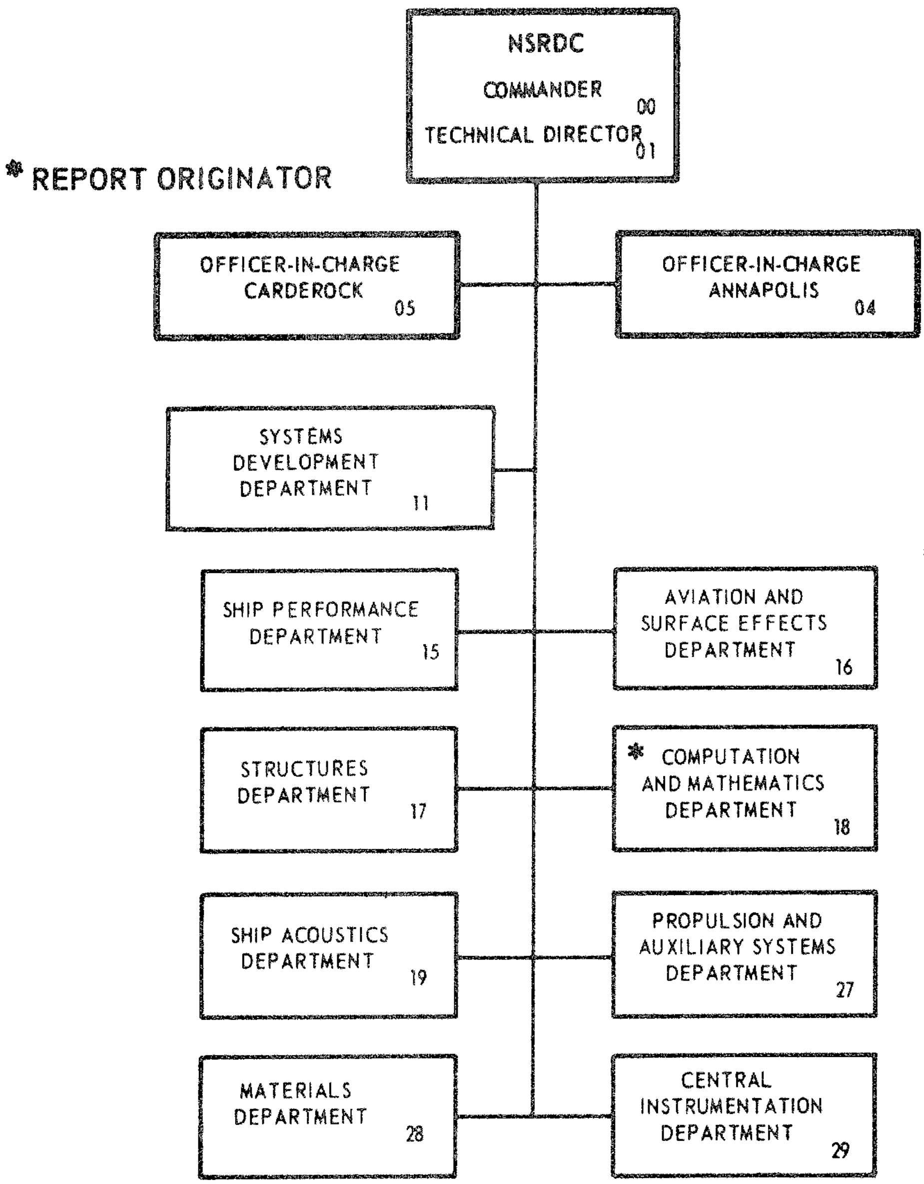

NDW-NSRDC 3960/44 (REV. 8/71)

GPO 917-872

DEPARTMENT OF THE NAVY
NAVAL SHIP RESEARCH AND DEVELOPMENT CENTER
Bethesda, Md. 20034

LAMINAR FLOW CIRCULATION IN A ROTATING TANK WITH A SPINNING COVER

by

Hans J. Lugt, Henry J. Haussling, Samuel Ohring

COMPUTATION AND MATHEMATICS DEPARTMENT

February 1972 Report 3797

TABLE OF CONTENTS

LIST OF FIGURES AND TABLES

Page

NOTATION

A, B, C, D, E	Abbreviations introduced in Equation (18)
a, b	Stretching factors defined by Equation (15)
c	Constant defined in Equation (29)
Ek	Ekman number
f	Frequency
H	Height of the tank
k	Summation index
$\vec{k}$	Unit vector in the direction of rotation
L	Radius of the tank
l, m	Eigenvalues
p'	Pressure
p	Dimensionless pressure
Ro	Rossby number
r', ϕ, z'	Cylindrical polar coordinates
r, ϕ, z	Dimensionless cylindrical polar coordinates
t'	Time
t	Dimensionless time
u', v', w'	Velocity components corresponding to r', ϕ, z'
u, v, w	Dimensionless velocity components
α, β	Abbreviations introduced in Equation (18)
γ_k	Abbreviation introduced in Equation (28)
δ	Ratio H/L
$\vec{\zeta}$	Dimensionless vorticity vector
ζ	Azimuthal component of $\vec{\zeta}$
η, θ	Stretched coordinates z, r

ν	Kinematic viscosity
ρ	Density
σ, τ	Abbreviations introduced in Equation (28)
ψ	Dimensionless stream function
χ_k	Function introduced in Equation (28)
Ω	Angular velocity of the tank
Ω_c	Angular velocity of the cover
ω	$= \Omega - \Omega_c$

Sub- and Superscripts:

i, j	Location of grid point in the (η, θ)-plane
n	Location of grid point in time

ABSTRACT

A study has been made of axisymmetric incompressible fluid flows in a rotating tank when the angular speed of the cover changes abruptly. From the initial solid-body rotation a meridional and an azimuthal circulation relative to the moving tank develop. This problem is solved numerically by means of a stream function-vorticity formulation for the meridional flow. Local fine grids are used in the Ekman and Stewartson layers. No finite gap between tank and cover is considered. The singular behavior at this point is investigated. The parameters considered are the Rossby number, the Ekman number, and the ratio of height to radius of the tank. Temporal and spatial oscillations of the laminar flow field as well as the occurrence of cell flows are discussed.

ADMINISTRATIVE INFORMATION

This study was supported by the Naval Ship Systems Command under the Mathematical Sciences Program, Subproject SR 003 03 01. An abridged version was presented at the IUTAM Symposium on Unsteady Boundary Layers, Laval University, Quebec, Canada, 25-29 May 1971 and was published in the Proceedings of the Symposium under the title "Transient Ekman and Stewartson Layers in a Rotating Tank with a Spinning Cover."

1. INTRODUCTION

In recent years the study of rotating fluids has found widespread interest from both the theoretical and practical point of view. Applications of this subject range from lubrication problems to centrifuge design to geophysical questions. Physically, rotating fluids can behave quite differently from nonrotating ones, a fact which has important mathematical implications. In the Computation and Mathematics Department the program to simulate viscous fluid flows by means of computers includes the study of rotating fluids. The present analysis is an outgrowth of this effort.

We consider the following laminar flow problem. A circular-cylindrical tank, completely filled with an incompressible fluid, is rotating around its axis with a constant angular velocity. The cover is a disk which can rotate co-axially with the tank but at a different rate. Initially, both tank and cover rotate with the same angular velocity, and the fluid inside behaves as a solid body. At a certain instant, the angular speed of the cover abruptly changes to a rate which is different from that of the tank. As a result, a meridional and an azimuthal circulation relative to the moving tank develop with time and approach asymptotically a steady state. A numerical computation of this flow is the subject of the present study.

A number of finite-difference solutions, obtained with the stream function-vorticity formulation for the meridional flow, have recently been published in the literature. Steady-state integrals for flows within a fixed tank with a spinning cover were found by Dorfman and Romanenko[1] and by Pao[2]. The steady motions in a

---

[1] References are listed on page 43.

rotating tank with a fixed cover were studied by Pao[3] and by Farris et al[4]. Pao[3] also computed the initial phase of the flows after the abrupt change of the cover's rotational speed. Flows with sources and sinks on the boundaries were investigated by Farris et al[4] for the steady-state case and by Krause[5] for the transient case. Small deviations from solid-body rotation allow the linearization of the equations of motion. This approach was chosen by Rasmussen[6]. The spin-up and spin-down of a cylindrical tank without relative rotation of the cover was studied by Briley and Walls[7].

A wealth of literature exists for limiting cases which permit similarity assumptions or the use of perturbation methods. The solutions obtained are valuable as a means of checking the accuracy of the numerical techniques. Older papers are recorded in Schlichting's book[8], newer papers in Greenspan's monograph[9]. In particular, attention is called to the paper by Pearson[10]. The spin-up and spin-down problems were studied by Greenspan[9] and by Euteneuer et al[11]. Details of some of the papers are discussed in context with our results.

The problem outlined in the beginning of this section is solved by means of a stream function-vorticity formulation. The numerical technique is essentially that presented by the authors in Reference 12. Grid systems of 41x41 = 1681 and 51x51 = 2601 mesh points with unequal spacing represent the flow field. Thus, local fine grids can be used in regions with high vorticity gradients. The parameters of the problem are the Rossby number Ro, Ekman number Ek, and the aspect ratio δ of the tank.

The assignment of values to these parameters is guided by the objective of studying flows in a tank with nonvanishing angular speed. It is of advantage to solve the equations of motion in a rotating frame when studying the elliptic or hyperbolic flow behavior in space or in time for small Rossby numbers. This can be seen immediately for the linearized case, Ro = 0. Then the nondimensional vorticity transport equation takes the form

$$\left(\frac{\partial^2}{\partial t^2} - 2\mathrm{Ek}\,\frac{\partial}{\partial t}\,\nabla^2 + \mathrm{Ek}^2\,\nabla^4\right)\nabla^2\,\vec{\zeta} + (2\vec{k}\cdot\nabla)^2\,\vec{\zeta} = 0\ ,$$

where $\vec{k}$ is the unit vector in the direction of rotation. The other quantities are described in Section 2. When Ek is small the hyperbolic form of the equation in time is revealed. For steady motions we arrive at the Taylor-Proudman theorem if Ek = 0[9].

2. FORMULATION OF THE INITIAL-BOUNDARY VALUE PROBLEM

We assume a laminar axisymmetric flow of an incompressible fluid in a circular-cylindrical tank of radius L and height H, which is spinning with constant angular velocity Ω. At time $t'=0$ the cover impulsively starts to rotate with a different but constant angular velocity Ω_c. Cylindrical polar coordinates r', ϕ, z' are used with the corresponding velocity components u', v', w' in a reference frame rotating with the tank. Under the restriction of axisymmetry, $\partial/\partial\phi \equiv 0$, the Navier-Stokes equations and the equation of continuity are

$$u'_{t'} + u'u'_{r'} + w'u'_{z'} - v'\left(2\Omega + \frac{v'}{r'}\right) = -\frac{1}{\rho}p'_{r'} + \nu\left[u'_{r'r'} + \left(\frac{u'}{r'}\right)_{r'} + u'_{z'z'}\right], \quad (1)$$

$$v'_{t'} + u'v'_{r'} + w'v'_{z'} + u'\left(2\Omega + \frac{v'}{r'}\right) = \nu\left[v'_{r'r'} + \left(\frac{v'}{r'}\right)_{r'} + v'_{z'z'}\right], \quad (2)$$

$$w'_{t'} + u'w'_{r'} + w'w'_{z'} = -\frac{1}{\rho} p'_{z'} + \nu\left[w'_{r'r'} + \frac{w'_{r'}}{r'} + w'_{z'z'} \right], \tag{3}$$

$$u'_{r'} + \frac{u'}{r'} + w'_{z'} = 0 . \tag{4}$$

Here, p', ρ, and ν are the pressure, the constant density, and the constant kinematic viscosity, respectively. Prior to the sudden change of rotation of the cover, the entire fluid is at rest relative to the spinning tank:

$$t' < 0: \quad u' \equiv 0, \quad v' \equiv 0, \quad w' \equiv 0 . \tag{5}$$

After the change of rotation, $t' \geq 0$, the boundary conditions are

$$\begin{aligned} &z' = 0,\ 0 \leq r' \leq L: \ u' = 0,\ v' = 0,\ w' = 0, \\ &z' = H,\ 0 \leq r' \leq L: \ u' = 0,\ v' = -\omega r',\ w' = 0, \\ &r' = L,\ 0 \leq z' < H: \ u' = 0,\ v' = 0,\ w' = 0 , \end{aligned} \tag{6}$$

where $\omega = \Omega - \Omega_c$. It is convenient to introduce the following dimensionless variables:

$$t' = t/\Omega, \quad r' = Lr, \quad z' = Hz, \quad (u', v') = \omega L(u, v), \quad w' = \omega H w, \quad p' = \rho\omega\Omega L^2 p \tag{7}$$

and the characteristic numbers

$$\begin{aligned} &Ro = \frac{\omega}{\Omega} &&\text{(Rossby number)}, \\ &Ek = \frac{\nu}{\Omega H^2} &&\text{(Ekman number)}, \\ &\delta = \frac{H}{L} &&\text{(aspect ratio)}, \end{aligned} \tag{8}$$

The axisymmetry of the motion permits the stream function-vorticity formulation of the meridional flow. If ψ designates the dimensionless stream function and ζ the azimuthal component of the dimensionless vorticity vector $\vec{\zeta}$, where

$$u = \frac{1}{r}\psi_z , \quad w = -\frac{1}{r}\psi_r , \tag{9}$$

$$\zeta = u_z - \delta^2 w_r , \tag{10}$$

Equations (1) through (4) are reduced to

$$\zeta_t + Ro[(u\zeta)_r + (w\zeta)_z - (\frac{v^2}{r})_z] - 2v_z = Ek[\delta^2(\zeta_{rr} + \frac{1}{r}\zeta_r - \frac{1}{r^2}\zeta) + \zeta_{zz}] , \tag{11}$$

$$v_t + Ro[(uv)_r + (wv)_z + 2\frac{uv}{r}] + 2u = Ek[\delta^2 (v_{rr} + \frac{1}{r}v_r - \frac{v}{r^2}) + v_{zz}] , \tag{12}$$

$$\frac{1}{r}[\delta^2 (\psi_{rr} - \frac{1}{r}\psi_r) + \psi_{zz}] = \zeta . \tag{13}$$

The corresponding boundary conditions for $t \geq 0$ are

$$\begin{array}{ll} z = 0,\ 0 \leq r \leq 1: & \psi = 0,\ \psi_z = 0,\ v = 0, \\ z = 1,\ 0 \leq r \leq 1: & \psi = 0,\ \psi_z = 0,\ v = -r, \\ r = 1,\ 0 \leq z < 1: & \psi = 0,\ \psi_r = 0,\ v = 0, \\ r = 0,\ 0 \leq z < 1: & \psi = 0,\ \zeta = 0,\ v = 0. \end{array} \tag{14}$$

The last conditions for the values on the centerline follow from the axisymmetry of the flow, which allows restriction to half the meridional plane.

At the corner $r = 1$, $z = 1$ a discontinuity in v occurs which causes the shear stresses $\lim_{r \to 1} \nu\rho(\frac{\partial v}{\partial z})_{z=1}$ and $\lim_{z \to 1} \nu\rho(\frac{\partial v}{\partial r})_{r=1}$ to be unbounded at that point. In reality, a small gap between cover and container always exists. Thus, this singularity is avoided. The matter was discussed by Schmieden[13] for slow motion with no meridional flow. If the gap is taken to be infinitesimal (as in this work), the torques exerted on the cover and the tank are always logarithmically singular. Although the singularity becomes more and more localized with decreasing Ekman number, the torques are always infinite. The implications for the finite-difference scheme are discussed below.

3. NUMERICAL INTEGRATION

For finite-difference techniques it is of advantage to lay out a network which is dense in regions of high vorticity gradients. Such regions usually occur as boundary layers near solid walls. For the present problem the following coordinate transformation is introduced:

$$\begin{aligned} r &= \theta + a \sin \pi \theta , \\ z &= \eta - b \sin 2\pi \eta , \end{aligned} \tag{15}$$

where the stretching factors a and b are chosen from the intervals $0 \le a \le 0.26$ and $0.10 \le b \le 0.13$. The region of integration is represented by a grid with mesh points at $\eta = \eta_i = (i-1)\Delta\eta$, $\theta = \theta_j = (j-1)\Delta\theta$, where $i, j = 1, \ldots, 41$ or 51. (See Figure 1.)

After the equations of motion are transformed according to Equation (15), they are solved with the following finite-difference scheme. The linear differential operators of Equations (11) and (12), except for the Coriolis terms, are replaced by the Dufort-Frankel approximation. The term $-2v_z$ and the nonlinear operators are expressed by central-difference formulae. Then, Equations (11)

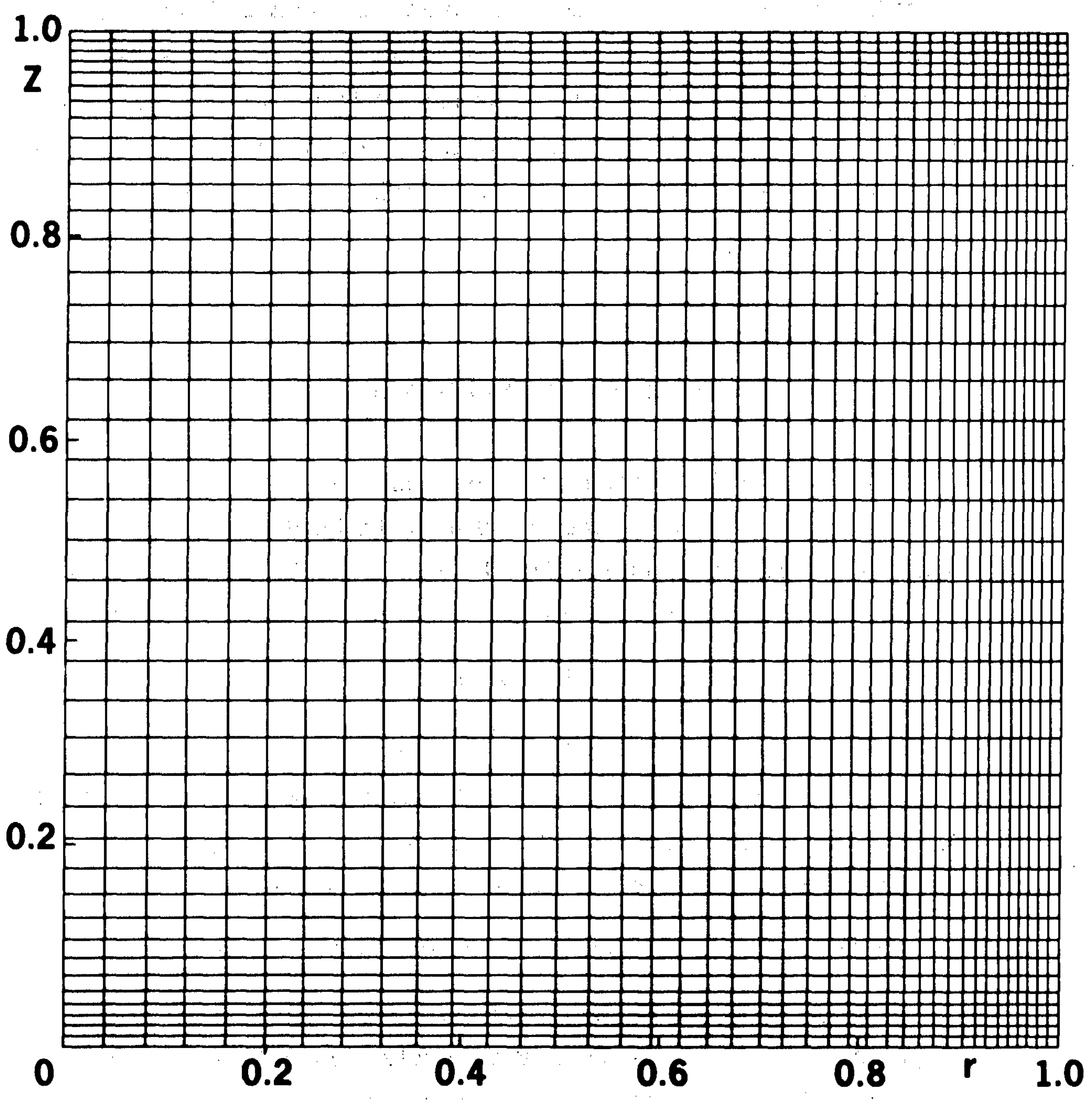

Figure 1 - Grid System with 41 x 41 Mesh Points and Stretching Factors a = 0.2, b = 0.1

and (12) yield, for the $(n+1)^{th}$ time step,

$$\zeta^{n+1}_{i,j} = (1-2E_k \Delta t C_{i,j})^{-1}\{\zeta^{n-1}_{i,j} + 2\Delta t\,[\mathrm{Ro}(\alpha_j \frac{u^n_{i,j-1}\zeta^n_{i,j-1} - u^n_{i,j+1}\zeta^n_{i,j+1}}{2\Delta\theta}$$

$$+ \beta_i \frac{w^n_{i-1,j}\zeta^n_{i-1,j} - w^n_{i+1,j}\zeta^n_{i+1,j}}{2\Delta\eta} + \frac{v^n_{i,j}}{r_j}\beta_i \frac{v^n_{i+1,j} - v^n_{i-1,j}}{\Delta\eta})$$

$$+ \beta_i \frac{v^n_{i+1,j} - v^n_{i-1,j}}{\Delta\eta} + E_k(A_j\zeta^n_{i,j+1} + B_j\zeta^n_{i,j-1} + C_{i,j}\zeta^{n-1}_{i,j}$$

$$+ D_i\zeta^n_{i+1,j} + E_i\zeta^n_{i-1,j})]\}\ , \tag{16}$$

$$v^{n+1}_{i,j} = (1-2E_k \Delta t C_{i,j})^{-1}\{v^{n-1}_{i,j} + 2\Delta t\,[\mathrm{Ro}(\alpha_j \frac{u^n_{i,j-1}v^n_{i,j-1} - u^n_{i,j+1}v^n_{i,j+1}}{2\Delta\theta}$$

$$+ \beta_i \frac{w^n_{i-1,j}v^n_{i-1,j} - w^n_{i+1,j}v^n_{i+1,j}}{2\Delta\eta} - \frac{2}{r_j} u^n_{i,j}v^n_{i,j}) - 2u_{i,j}$$

$$+ E_k(A_j v^n_{i,j+1} + B_j v^n_{i,j-1} + C_{i,j}v^{n-1}_{i,j} + D_i v^n_{i+1,j} + E_i v^n_{i-1,j})]\}\ . \tag{17}$$

Here, the following abbreviations are used:

$$\alpha_j \equiv \frac{1}{1+a\pi\cos\pi\theta_j}\ , \qquad \beta_i \equiv \frac{1}{1-2\pi b\cos 2\pi\eta_i}\ ,$$

$$r_j \equiv \theta_j + a\sin\pi\theta_j\ ,$$

$$A_j \equiv (\frac{\delta\alpha_j}{\Delta\theta})^2 + \frac{\pi^2\delta^2\alpha_j^3\, a\sin\pi\theta_j}{2\Delta\theta} + \frac{\delta^2\alpha_j}{2r_j\Delta\theta}\ ,$$

$$B_j \equiv (\frac{\delta\alpha_j}{\Delta\theta})^2 - \frac{\pi^2\delta^2\alpha_j^3\, a\sin\pi\theta_j}{2\Delta\theta} - \frac{\delta^2\alpha_j}{2r_j\Delta\theta}\ ,$$

$$C_{i,j} \equiv -\left(\frac{\delta\alpha_j}{\Delta\theta}\right)^2 - \frac{\delta^2}{2r_j^2} - \left(\frac{\beta_i}{\Delta\eta}\right)^2 ,$$

$$D_i \equiv \left(\frac{\beta_i}{\Delta\eta}\right)^2 - \frac{2\pi^2 \beta_i^3 b \sin 2\pi\eta_i}{\Delta\eta} ,$$

$$E_i \equiv \left(\frac{\beta_i}{\Delta\eta}\right)^2 + \frac{2\pi^2 \beta_i^3 b \sin 2\pi\eta_i}{\Delta\eta} . \tag{18}$$

The velocity components of the meridional flow are obtained from

$$u_{i,j} = \frac{\beta_i}{r_j} \frac{\psi_{i+1,j} - \psi_{i-1,j}}{2\Delta\eta} , \quad w_{i,j} = -\frac{\alpha_j}{r_j} \frac{\psi_{i,j+1} - \psi_{i,j-1}}{2\Delta\theta} . \tag{19}$$

The Poisson-type Equation (13) is approximated by the five-point formula which yields, for $\psi_{i,j}$,

$$\psi_{i,j} = \frac{1}{2}\left[\left(\frac{\delta\alpha_j}{\Delta\eta}\right)^2 + \left(\frac{\beta_i}{\Delta\eta}\right)^2\right]^{-1} \left[D_i \psi_{i+1,j} + E_i \psi_{i-1,j}\right.$$

$$\left. + \left(A_j - \frac{\delta^2\alpha_j}{r_j\Delta\theta}\right)\psi_{i,j+1} + \left(B_j + \frac{\delta^2\alpha_j}{r_j\Delta\theta}\right)\psi_{i,j-1} - r_j\zeta_{i,j}\right] . \tag{20}$$

This system of algebraic equations is solved with Gauss-Seidel line overrelaxation applied along lines of constant θ. The overrelaxation factor is 1.78. The iteration is halted after the k^{th} iteration if, at each grid point,

$$|\psi_{i,j}^{k} - \psi_{i,j}^{k-1}| < 10^{-4} |\psi_{i,j}^{k-1}| . \tag{21}$$

At the solid boundaries a one-sided first order difference equation is used to compute the vorticity ζ. Two such equations were tried, the simple one which is used by most authors (at the bottom of the tank, for instance),

$$\zeta_{1,j} = \frac{2}{r_j}\left(\frac{\beta_1}{\Delta\eta}\right)^2 \psi_{2,j} \tag{22}$$

and another, which was found in a study involving curved boundaries[12] to be superior with regard to numerical stability,

$$\zeta_{1,j} = \frac{1}{4r_j}\left(\frac{\beta_1}{\Delta\eta}\right)^2 (\psi_{2,j} + 4\psi_{3,j} - \psi_{4,j}) \,. \tag{23}$$

In this paper Equation (23) is used although it showed no advantage over Equation (22).

It can be seen from Equations (16) through (20) and Equation (23) that the computations at the inner points do not require knowledge of quantities at the singular point. (The subscript $i+1, j+1$ does not appear in these equations.)

The integration process is carried out in the following way: The vorticity $\zeta_{i,j}^{n+1}$ and subsequently the azimuthal velocity $v_{i,j}^{n+1}$ are computed at the inner points according to Equations (16) and (17). The calculation of $\psi_{i,j}^{n+1}$ follows with the aid of Equation (20). The cycle then concludes with the calculation of the surface vorticity.

The maximum stable time step, Δt_{max}, beyond which numerical instability occurs, is determined by increasing the time step until oscillations from point to point in the ζ-values appear.

The accuracy of the computations is checked by using different space increments. This is easily done by varying the stretching parameters a and b defined in Equation (15). It is found for the two cases $Ro = 1$, $\delta = 1$, $Ek = 0.01$ and 0.001 that solutions obtained with different stretching values agree well except near the singular point. The influence of this singularity on the solution is discussed in Section 4. Another way to change the space increments is to vary the number of grid points. For $Ro = 1$, $Ek = 0.001$ two grid systems, 41 x 41 and 51 x 51, are used. The agreement is good.

4. RESULTS

As already noted, our main interest is focused on fluid motions in a rotating tank, that is flows with $Ro < \infty$. The examples selected for computation are compiled in Table 1. All cases are started from solid-body rotation at $t = 0$ and are continued to an almost steady state at t_{Final}, where t_{Final} is the earliest time at which

$$|\psi_{i,j}^{n} - \psi_{i,j}^{n-1}| \leq 10^{-4} |\psi_{i,j}^{n-1}| \tag{24}$$

is satisfied throughout the field. The computations were performed in double precision on an IBM 360-91 computer and in single precision on a CDC 6700 computer. Pictures of the flow field were made with a Stromberg- Carlson SC-4020 charactron plotter.

a. The Almost Steady Case

Two cases may be distinguished if the nonlinear inertial terms are neglibible. For large Ekman numbers the pressure force is essentially balanced only by the friction force (slow motion). For $Ro \ll Ek \ll 1$ a balance is maintained among the Coriolis, friction, and pressure forces.

Slow-motion solutions have been obtained by Hort[14] for $Ro = 1$, $\delta = 1$, $Ek = \infty$. Pao[3] checked numerically for $Ro = 1$, $\delta = 1$ that the

TABLE 1

Compilation of the Calculated Examples

No.	Ro	Ek	δ	a	b	GRID
1	10^{-5}	0.01	1	0.2	0.1	41 x 41
2	10^{-5}	0.001	1	0.2	0.1	
3	10^{-4}	0.01	1	0.2	0.1	
4	1	0.01	1	0.0	0.1	
5	1	0.01	1	0.26	0.13	
6	1	0.005	1	0.15	0.1	
7	1	0.0025	1	0.2	0.1	
8	1	0.00125	1	0.2	0.1	
9	1	0.001	1	0.2	0.1	
10	1	0.001	1	0.26	0.13	
11	1	0.001	1	0.0	0.0	51 x 51
12	1	0.0002	1	0.2	0.1	51 x 51
13	1	0.01	3	0.0	0.1	41 x 41
14	1	0.001	3	0.2	0.1	
15	1	0.01	1/2	0.2	0.1	
16	1	0.01	1/3	0.2	0.1	
17	4	0.01	1	0.2	0.1	
18	4	0.004	1	0.2	0.1	
19	10	0.01	1	0.2	0.1	

slow-motion approximation is applicable for $0.125 < Ek \leq \infty$.

The linear theory predicts for the case $Ro \ll Ek \ll 1$ three distinct regions: The Ekman layers at the cover and at the bottom of the tank, the Stewartson layer at the side wall, and the geostrophic interior, for which the Taylor-Proudman theorem of inviscid fluids holds[16]. Numerical results verify this notion and reveal its limitation. Figure 2 shows lines of constant ψ, ζ, and v-values for $Ro = 10^{-4}$, $Ek = 0.01$, $\delta = 1$ and for $Ro = 10^{-5}$, $Ek = 0.001$, $\delta = 1$. The increments of the ψ, ζ, and v-values are recorded in Table 2. The case $Ro = 10^{-5}$, $Ek = 0.001$, in particular the lines of constant ζ, illustrates clearly the existence of the three regions predicted by the linear theory. Additional results obtained for $Ro = 10^{-5}$, $Ek = 0.01$, $\delta = 1$ agree so well with the case $Ro = 10^{-4}$, $Ek = 0.01$, $\delta = 1$ that the patterns are indistinguishable. The increase of the Ekman number from 0.001 to 0.01 shows that the (almost) inviscid interior has vanished. If we neglect the influence of the side wall, an analytic solution from the linear theory is available. This is the well-known Ekman solution. In Figure 3 the numerical values for v at the centerline $r = 0$ are compared with those of the Ekman solution. Again, the analytic values agree well with the numerical output for $Ek = 0.001$, whereas for $Ek = 0.01$ the numerical data reveal the influence of the side wall. A distinct asymmetry is displayed between cover and bottom for $Ek = 0.01$.

The Stewartson layer at the side wall is studied with a perturbation method[9] and compared with the numerical output. Two different layers, one inside the other, must be distinguished: a layer of thickness $Ek^{1/4}$, and a layer of thickness $Ek^{1/3}$ inside the first layer and adjacent to the wall. The $Ek^{1/4}$-layer is represented

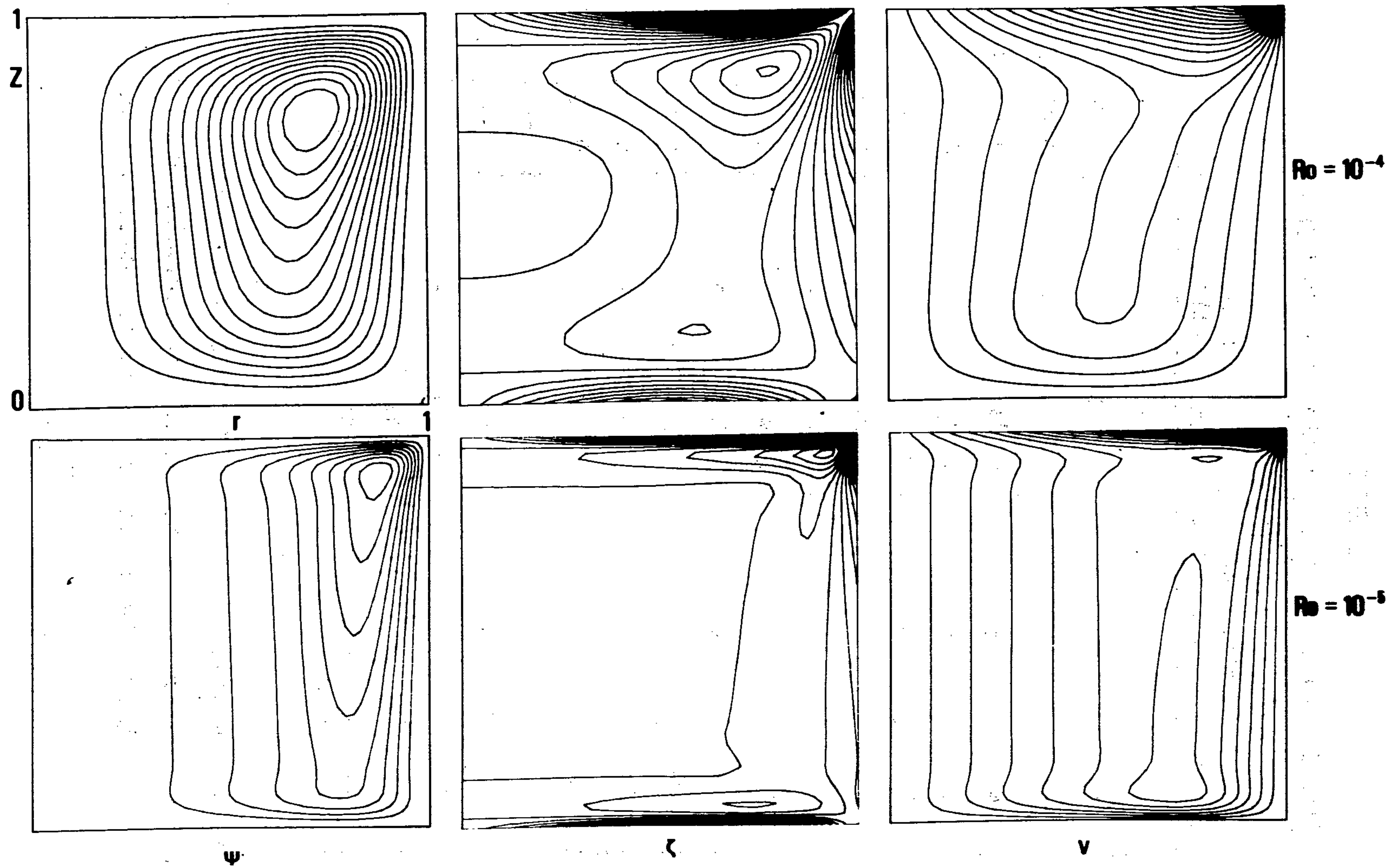

Figure 2 - Lines of constant ψ, ζ and v for $\delta = 1$, Ro = 10^{-4}, Ek = 0.01 and Ro = 10^{-5}, EK = 0.001 at almost Steady State

TABLE 2

Data for the ψ, ζ, and v Patterns in the Figures

No.	Figure	Sign of ψ Near r=1, z=1	$\Delta\psi$	Sign of ζ on the Cover	$\Delta\zeta$	Δv
2	2	-	0.001	-	1.00	0.05
3	2	-	0.001	-	0.25	0.05
5	6	-	0.001	-	0.25	0.05
7	6	-	0.001	-	0.25	0.05
8	7	-	0.001	-	0.50	0.05
10	7	-	0.001	-	0.50	0.05
12	8	-	0.001	-	1.00	0.05
19	8	+	0.001	+	0.50	0.05
17	9	+	0.001	+	0.25	0.05
18	9	+	0.001	+	0.25	0.05
13	10	-	0.0001	-	0.25	0.05
16	10	-	0.001	-	0.25	0.05
14	11	-	0.001	-	0.50	0.05
2	15	-	0.001	-	--	0.05
10	19	-	0.001	-	--	0.05
12	20	-	0.001	-	--	--
12	21	-	0.001	-	--	0.05
19	22	+	0.001	+	0.50	0.05

The stream function ψ is specified to be zero at the boundaries. The vorticity ζ is zero on the centerline. The azimuthal velocity v is zero at all boundaries except at the cover, where $v = -r$.

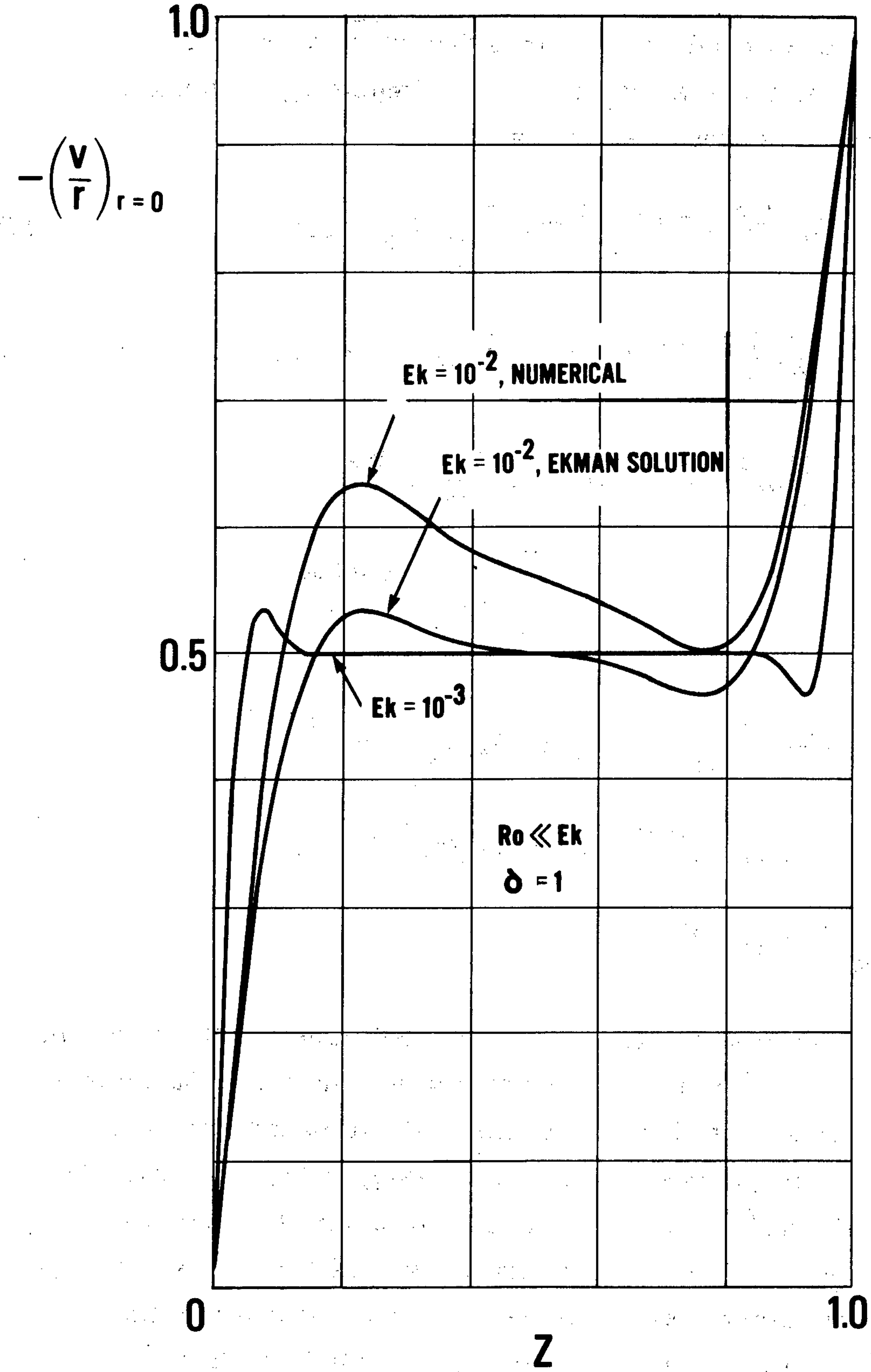

Figure 3 - Comparison of the Ekman Solution with the Numerical Results. $-(v/r)_{r=0}$ is Plotted versus z.

by a closed-form solution, whereas the $Ek^{1/3}$-layer must be expressed by a series expansion. For simplicity, the velocity components are presented for $\delta = 1$:

$$u = \frac{1}{2} Ek^{1/2} \, e^{-\sqrt{2}\,\sigma} - \frac{1}{2} Ek^{1/2} \sum_{k=1}^{\infty} (\chi_k)_{\tau\tau} \cos k\pi z \, , \tag{25}$$

$$v = -\frac{r}{2} + \frac{1}{2} e^{-\sqrt{2}\,\sigma} + Ek^{1/6} \sum_{k=1}^{\infty} \chi_k \cos k\pi z \, , \tag{26}$$

$$w = -\frac{1}{2} Ek^{1/2} - \frac{1}{\sqrt{2}} Ek^{1/4} \left(z - \frac{1}{2}\right) e^{-\sqrt{2}\,\sigma} + Ek^{1/6} \sum_{k=1}^{\infty} \chi_k \sin k\pi z \, , \tag{27}$$

where

$$\chi_k = (-1)^k \frac{2}{\sqrt{3}\, k\pi} \gamma_k \sin\left(\frac{\sqrt{3}}{2} \gamma_k \tau\right) e^{-\gamma_k/2 \, \tau} \, ,$$

$$\sigma = (1-r)/Ek^{1/4} \, , \quad \tau = (1-r)/Ek^{1/3} \, ,$$

$$\gamma_k = (2k\pi)^{1/3} \, . \tag{28}$$

The first term in v and w is the geostrophic mode of the interior. In Figures 4 and 5 the v- and w-components are plotted against r. The numerical results are compared with the analytic data for a) the geostrophic mode and the $Ek^{1/4}$-law, and b) the geostrophic mode, the $Ek^{1/4}$-law, and the first two nonzero terms of the $Ek^{1/3}$-series. For the v-component both analytic curves are in good agreement with the numerical data. For the w-component the $Ek^{1/4}$-law alone is insufficient to describe the Stewartson layer. In

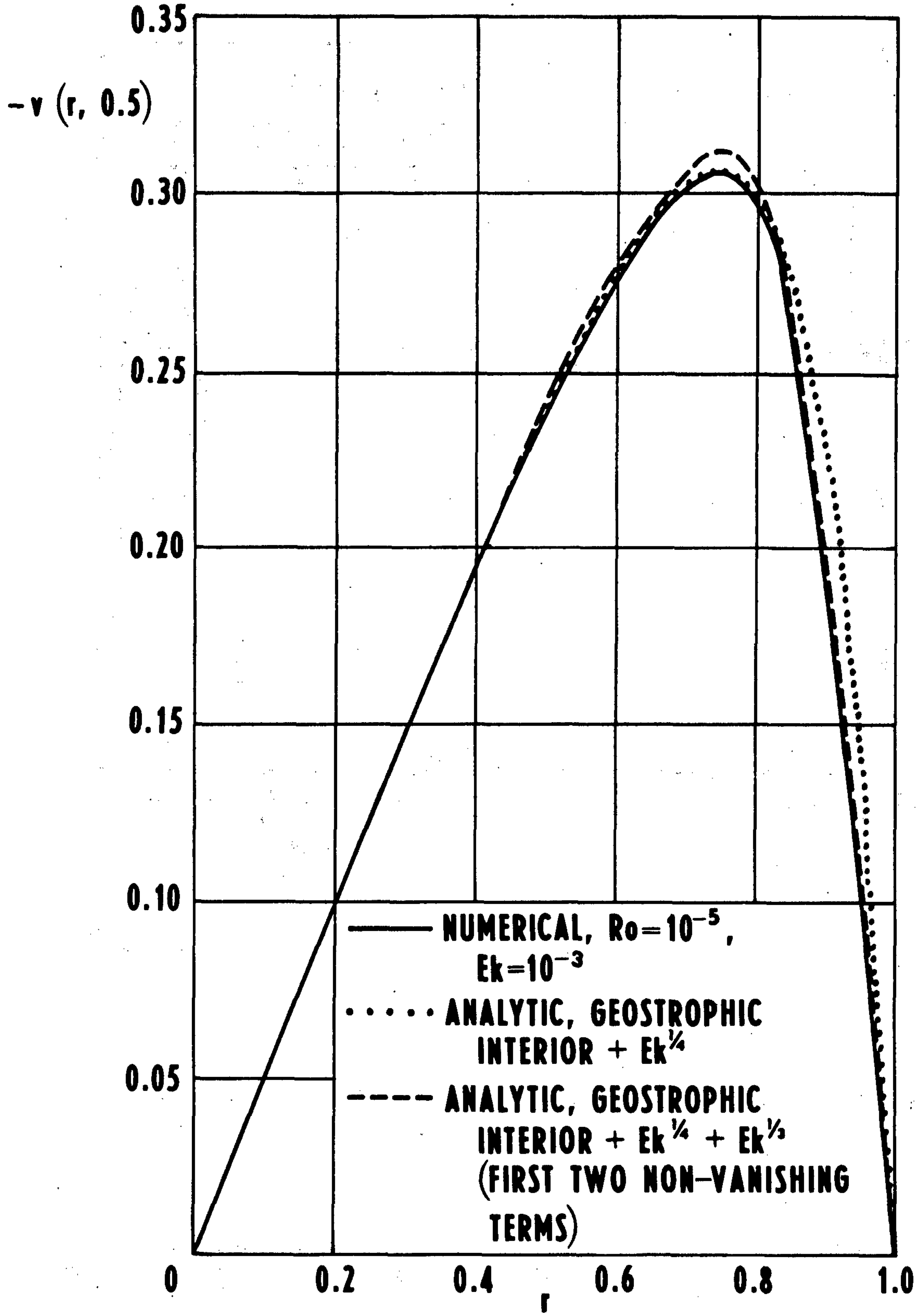

Figure 4 - Analytic and Numerical Results for the Stewartson Layer. $-v$ is Plotted Versus r at $z = 1/2$

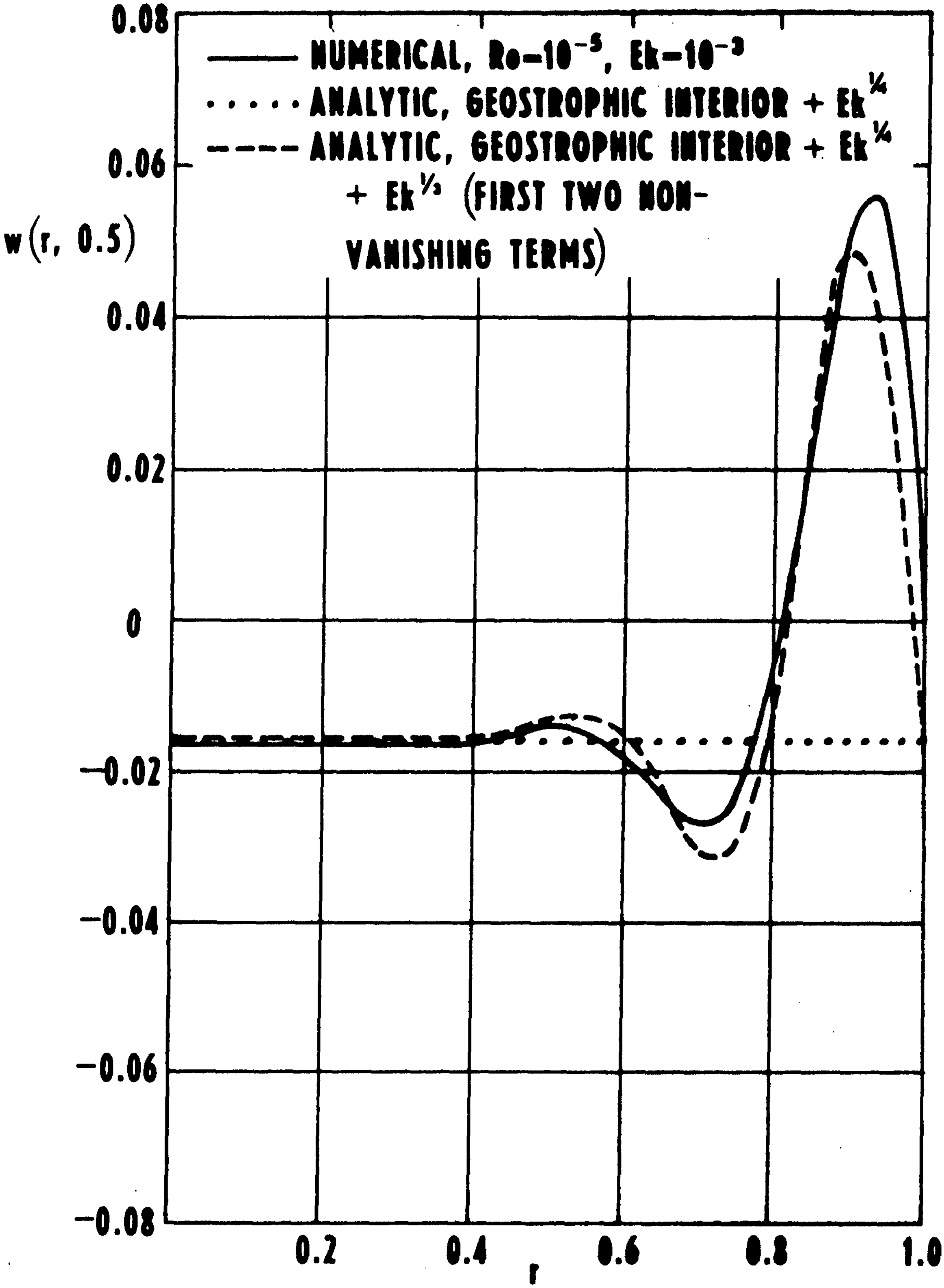

Figure 5 - Analytic and Numerical Results for the Stewartson Layer. w is Plotted Versus r at z = 1/2

fact, at $z = \frac{1}{2}$, the contribution of the $Ek^{1/4}$-law vanishes.

The inclusion of the nonlinear terms into the equations of motion modifies the flow characteristics. Figures 6 through 8 show flow patterns for Ro = 1, $\delta = 1$, and various Ek. The output for Ek = 0.01 can be compared with Pao's computation[3]. The overall streamline patterns agree well with each other, although deviations occur near the singular point. This problem is discussed in more detail below. In Figures 8 and 9 flow patterns are displayed for Ro = 10 and 4, $\delta = 1$, and two different Ekman numbers. Cell-type motions occur which are expected around Ro = 4 according to similarity solutions[17]. Results in Figures 10 through 12 exhibit the effect of various δ. In the limit $\delta \rightarrow 0$ the solutions approach the similarity solutions obtained by Lance and Rogers[15]. This is demonstrated in Figure 12 by a graph of $-v/r$ versus z at $r = 0$.

The results for different Ro, Ek, δ have one common feature. Below a certain value of the Ekman number, spatial undulations of the streamlines occur indicating the transition from an elliptic-type to a hyperbolic-type solution. This distinction is most apparent in the two linear cases discussed at the beginning of this section. The slow-motion solution is clearly elliptic, whereas the Ekman solution and the geostrophic mode are parabolic (as an asymptotic limit of the hyperbolic time-dependent flow). For Ro = 1, $\delta = 1$ the critical Ekman number, at which the transition occurs, is 0.005. This value decreases for Ro > 1 and increases for Ro < 1. Variation of δ appears to have only a minor effect on the value of the critical Ekman number.

In Figure 13 a pathline is displayed for Ro = 1, Ek = 0.0002, $\delta = 1$ in the rotating frame. The starting point is arbitrarily chosen at $r = 0.489$, $z = 0.959$. The fluid particle follows a trajectory which

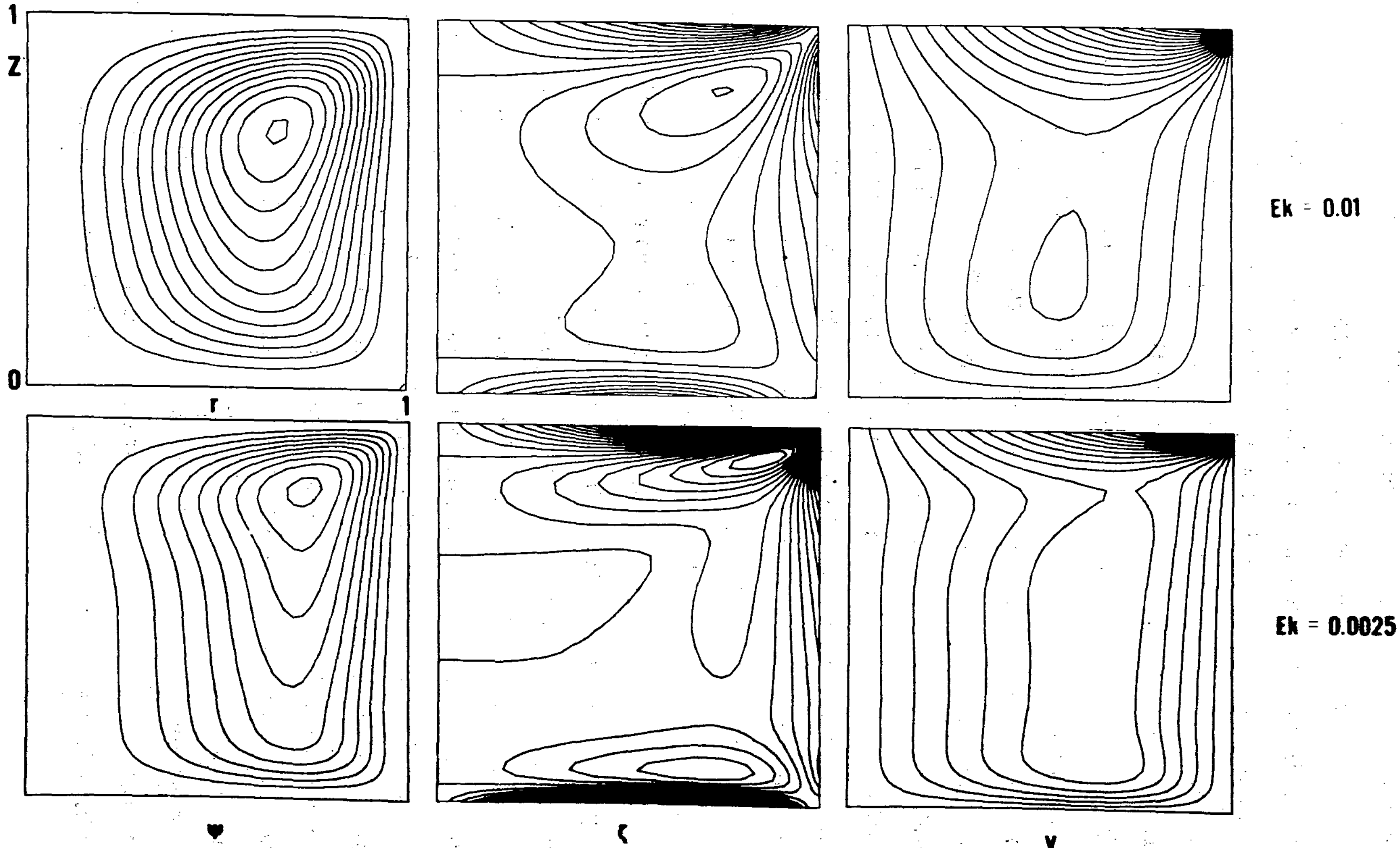

Figure 6 - Lines of Constant ψ, ζ, and v for Ro = 1, δ = 1, Ek = 0.01 and Ek = 0.0025 at almost Steady State

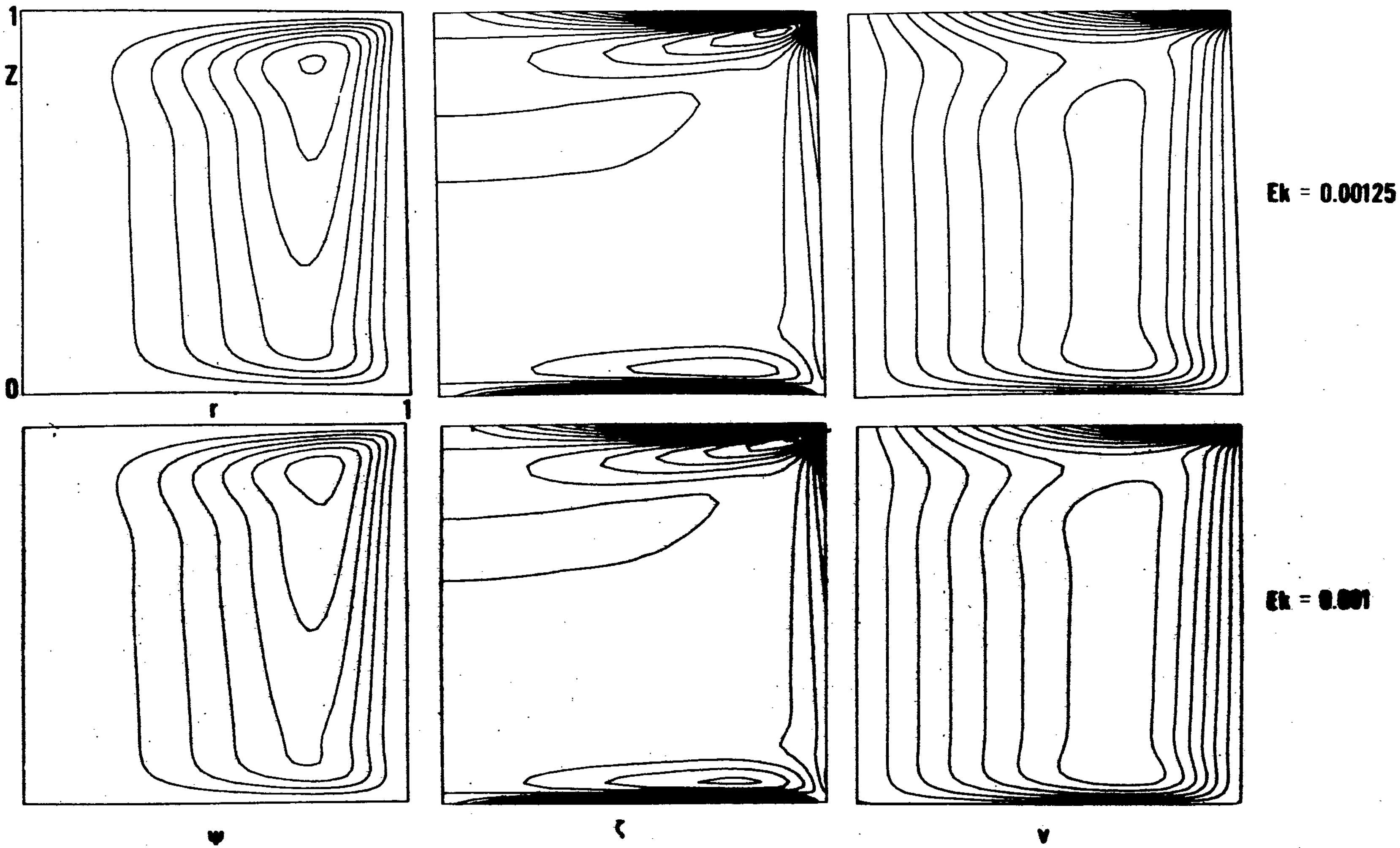

Figure 7 - Lines of Constant ψ, ζ, and v for Ro = 1, δ = 1, Ek = 0.00125 and Ek = 0.001 at almost Steady State

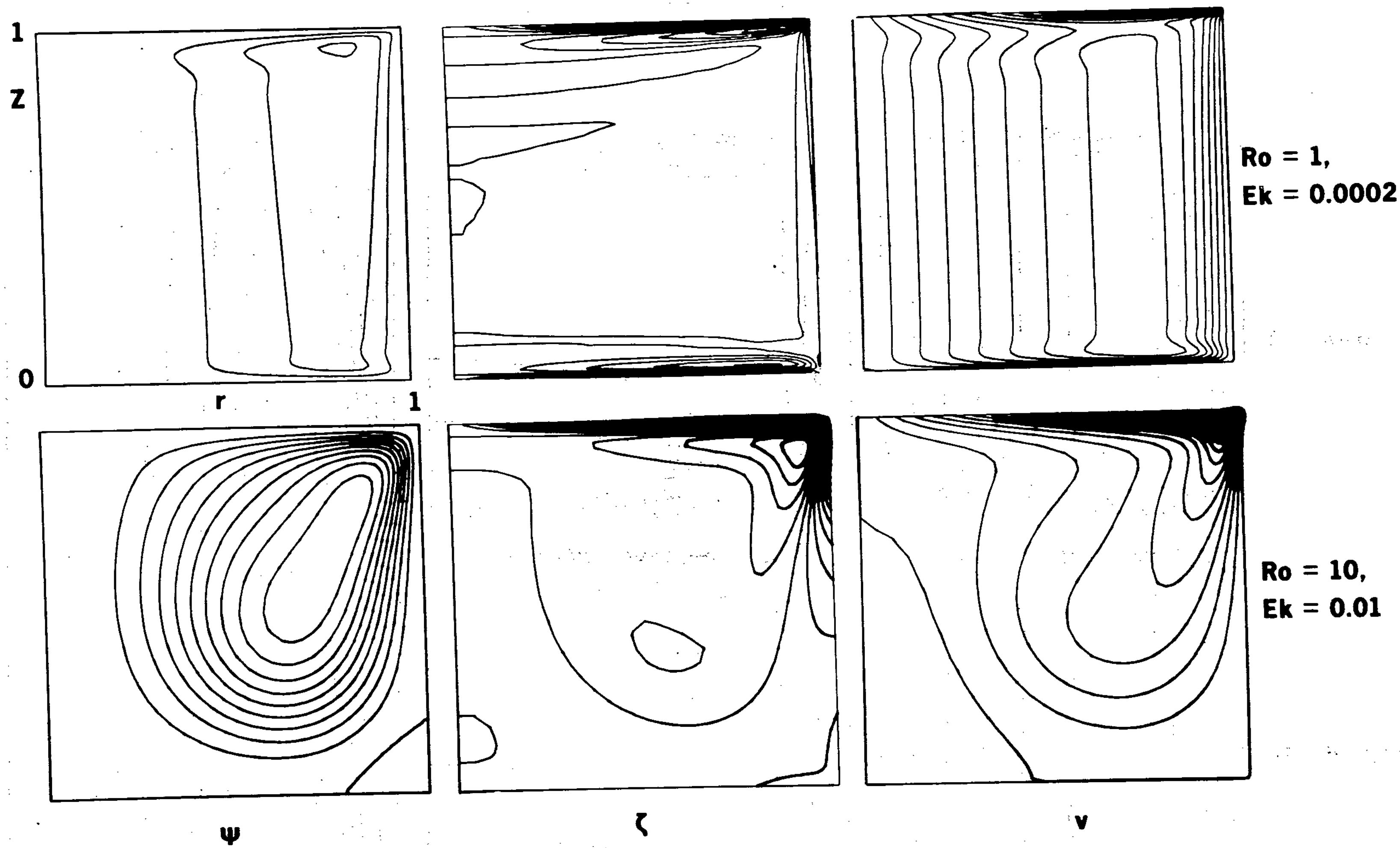

Figure 8 - Lines of Constant ψ, ζ, and v for Ro = 1, δ = 1, Ek = 0.0002 and Ro = 10, δ = 1, Ek = 0.01 at almost Steady State

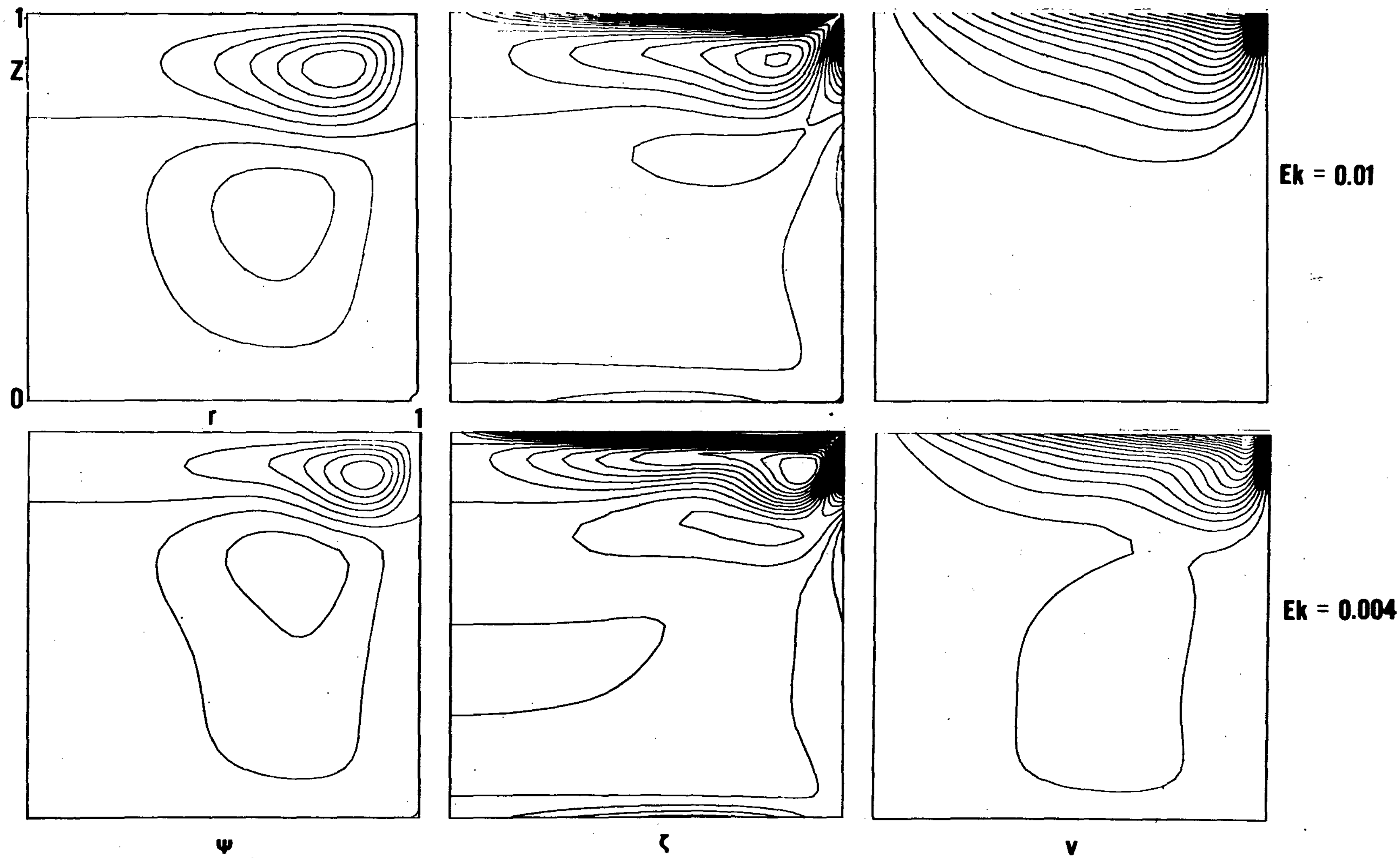

Figure 9 - Lines of Constant ψ, ζ, and v for Ro = 4, δ = 1, Ek = 0.01 and Ek = 0.004 at almost Steady State

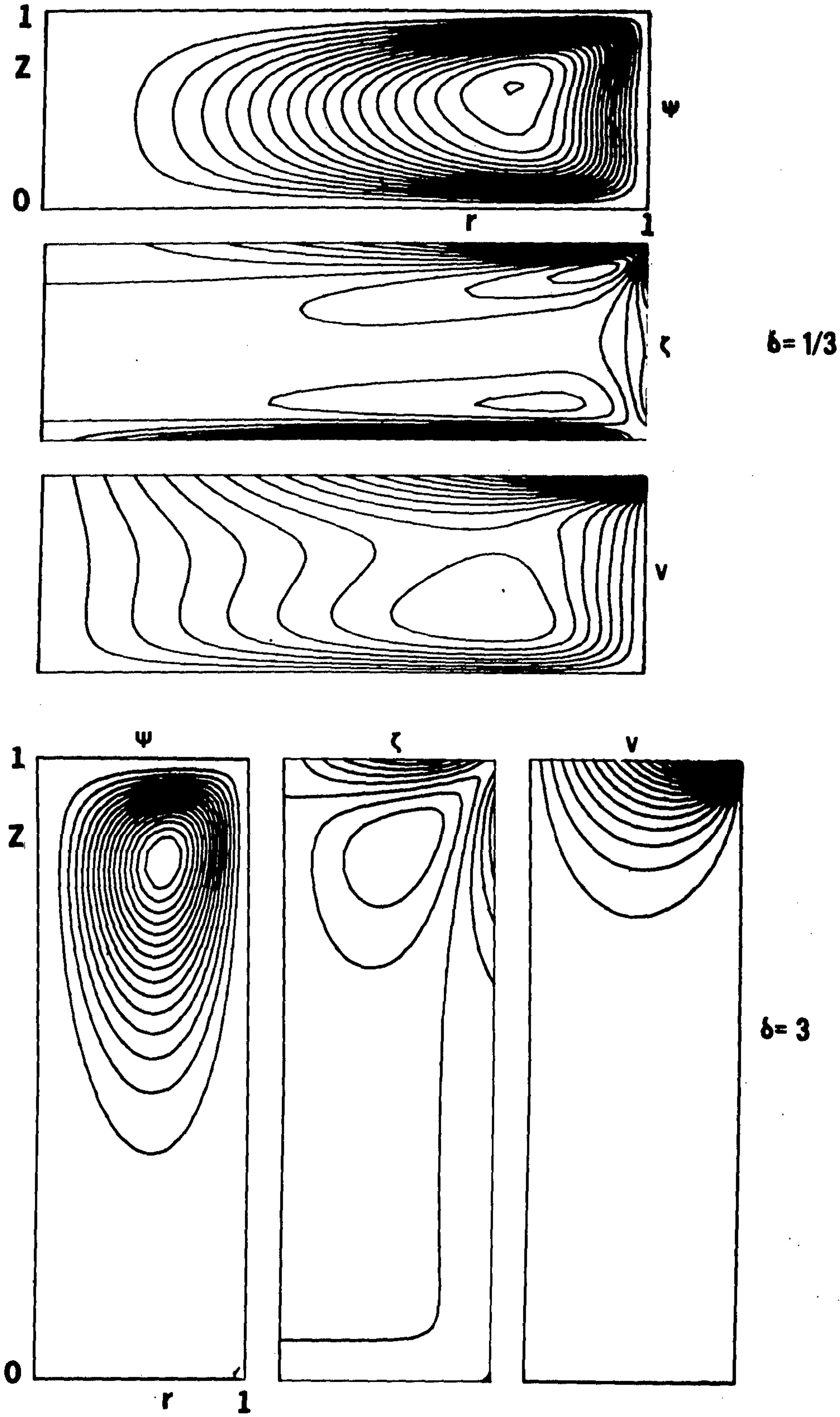

Figure 10 - Lines of Constant ψ, ζ, and v for Ro = 1, Ek = 0.01, δ = 3 and δ = 1/3 at almost Steady State

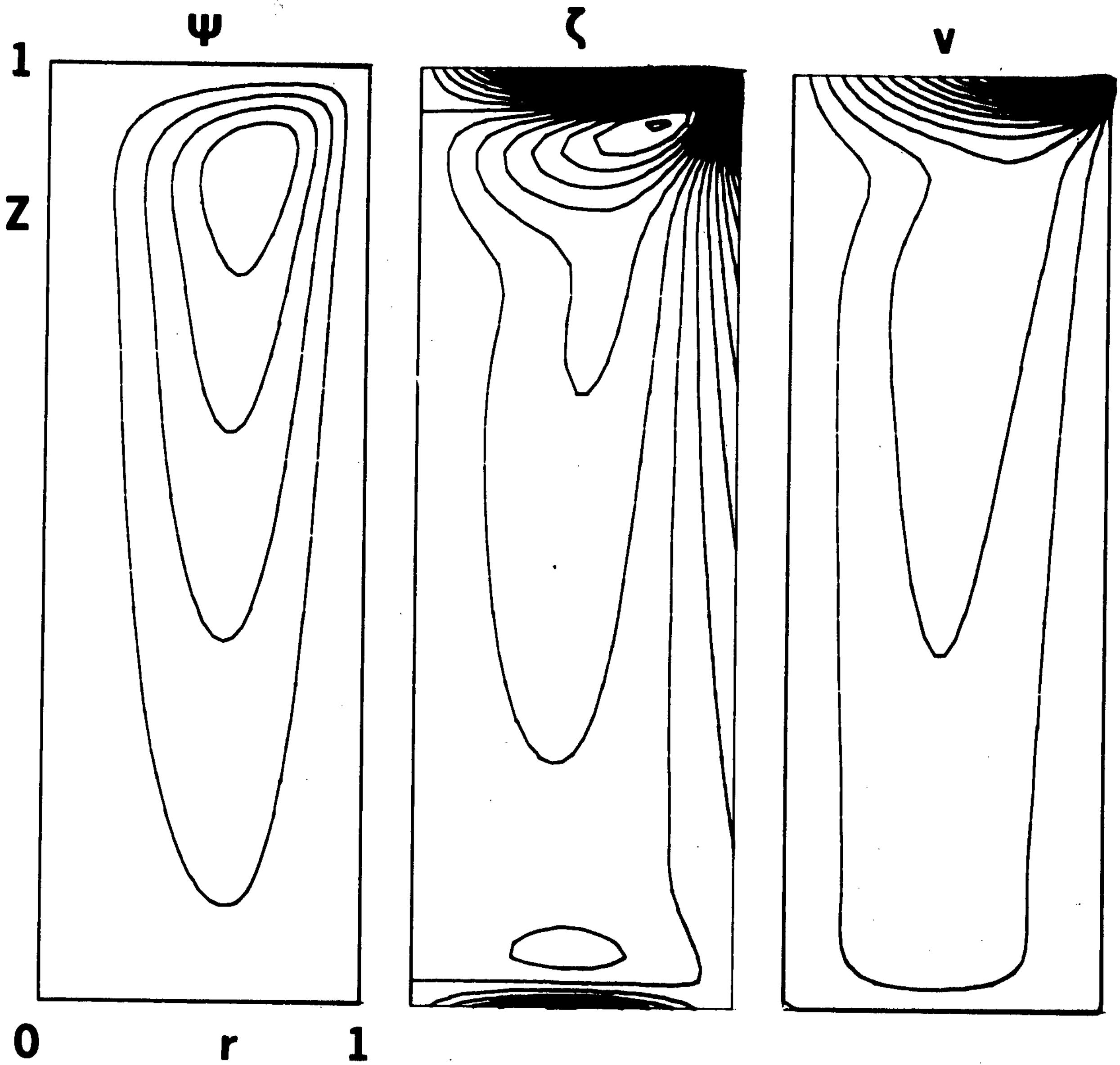

Figure 11 - Lines of Constant ψ, ζ, and v for Ro = 1, Ek = 0.001, δ = 3
at almost Steady State

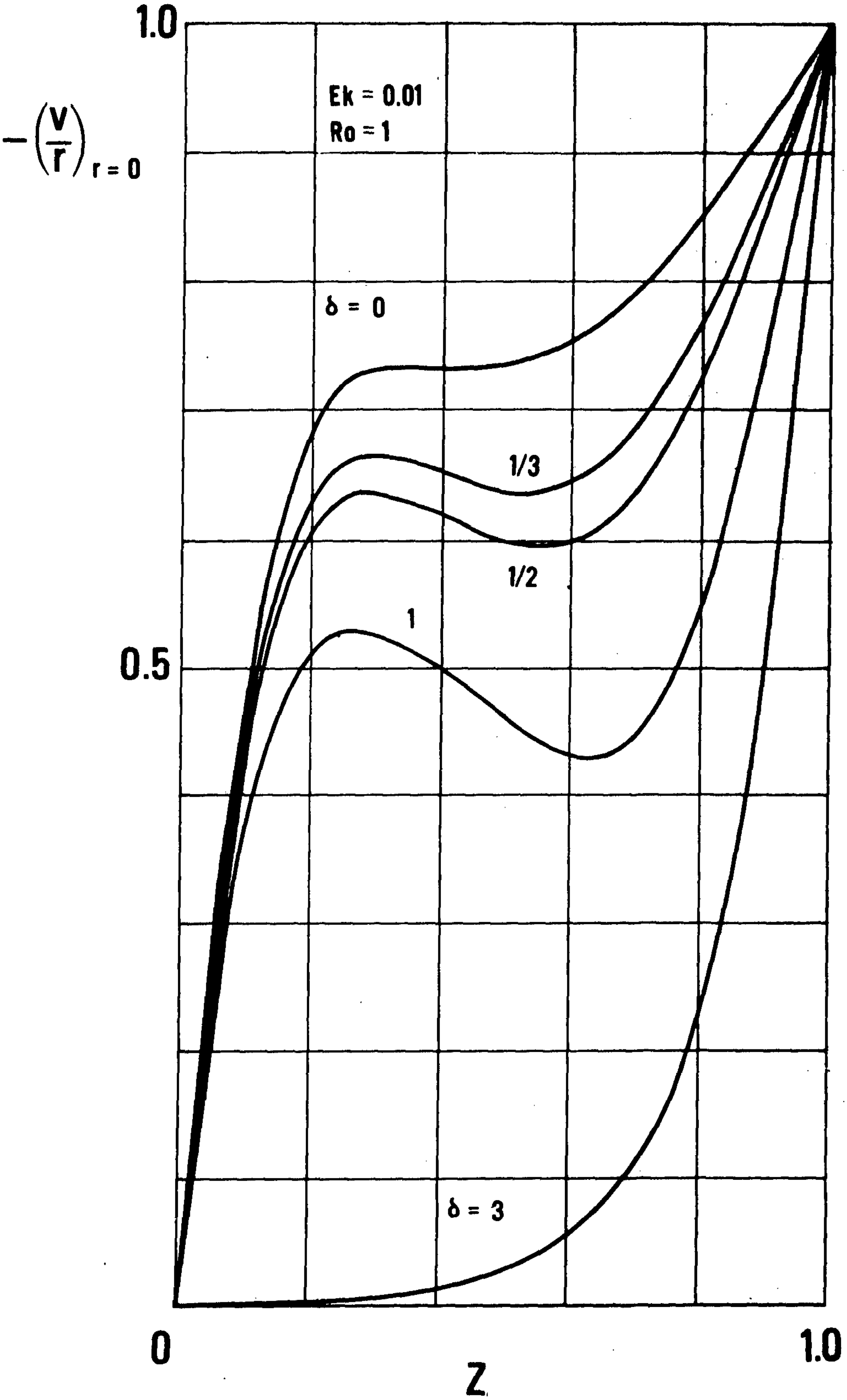

Figure 12 - $-(v/r)_{r=0}$ as a Function of z for Various δ

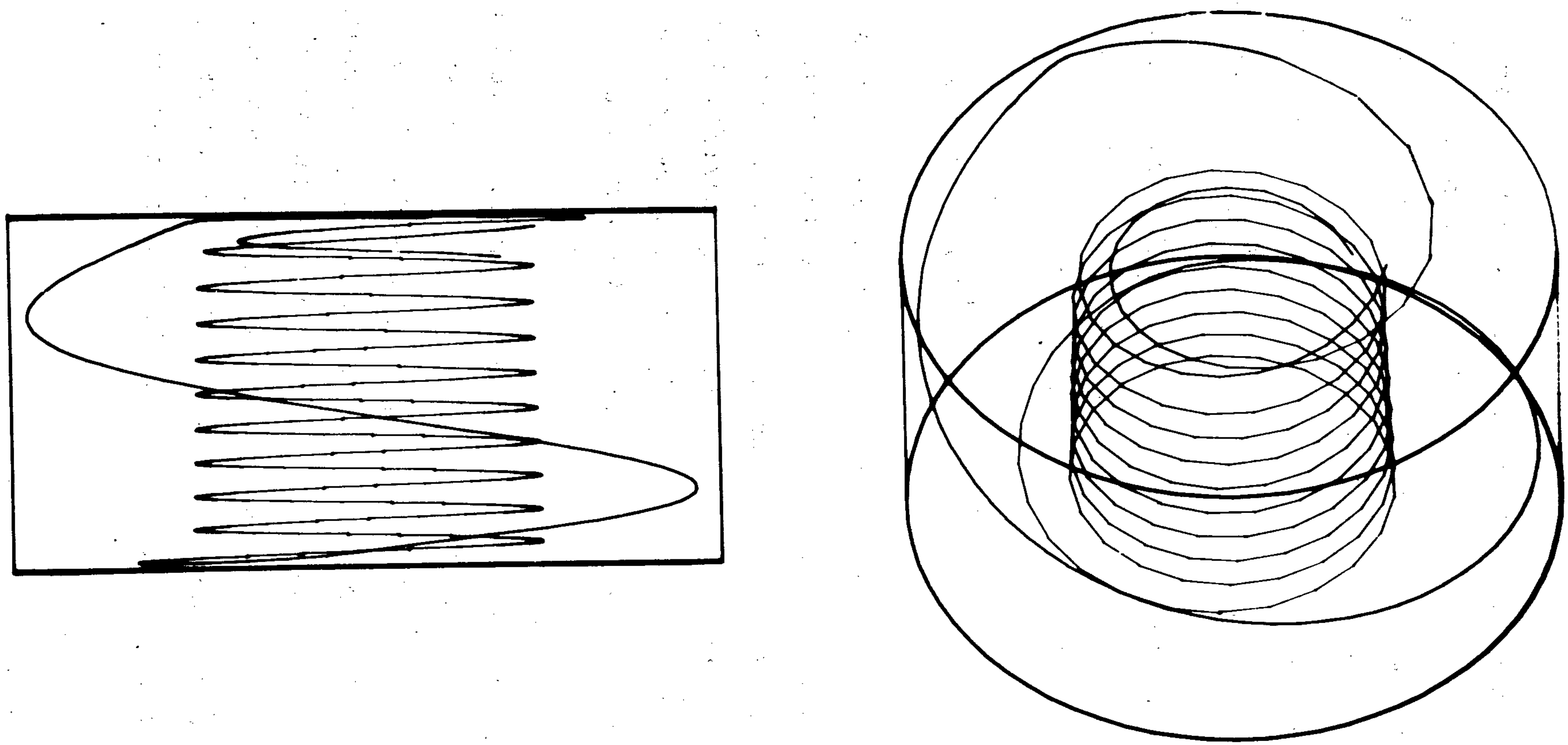

Figure 13 - Pathline for Ro = 1, Ek = 0.0002, δ = 1. Perspective View at almost Steady State

consists of a downward spiral with almost no radial variation and an upward spiral near the side wall with only one revolution. The time for the particle to return to the vicinity of its initial position is about 22 revolutions of the tank ($t = 140$).

The singularity of the flow at $r = 1$, $z = 1$ requires special attention. In Figure 14 the function $-\frac{1}{r}\left(\frac{\partial v}{\partial z}\right)_{z=1}$ is plotted against $(1-r)$ on a double-logarithmic scale for various values of Ro, Ek, and δ. The dimensional quantity $\partial v'/\partial z'$ becomes unbounded at the singular point ($r' = L$, $z' = H$) according to

$$\lim_{r' \to L} -\left(\frac{\partial v'}{\partial z'}\right)_{z'=H} = c\,\frac{L\omega}{L-r'}\,, \quad c \approx 0.73\,, \tag{29}$$

where c does not depend on Ro, Ek, or δ. Hence, the singularity is a local effect which can be considered in a numerical scheme by building in a local series expansion. On the other hand, the torques exerted on the cover and the wall are always logarithmically singular. Figure 14 reveals that for $Ro = 1$, $Ek = 0.01$ the grid system with $a = 0$, $b = 0.1$ gives a poor representation of the near-corner region.

b. The Transient Case

Unsteady rotating flows exhibit parabolic or hyperbolic properties in time. The slow-motion solution[14], for example, is a pure diffusion process and is, thus, parabolic. The linear theory of inviscid flow, in which the pressure gradient, the Coriolis force, and the local acceleration balance each other, reveals flows of hyperbolic nature[9]. This can be seen immediately for the vorticity equation cited in the introduction. If $Ek = 0$, an infinite but countable number of modes can be obtained. Their frequencies are

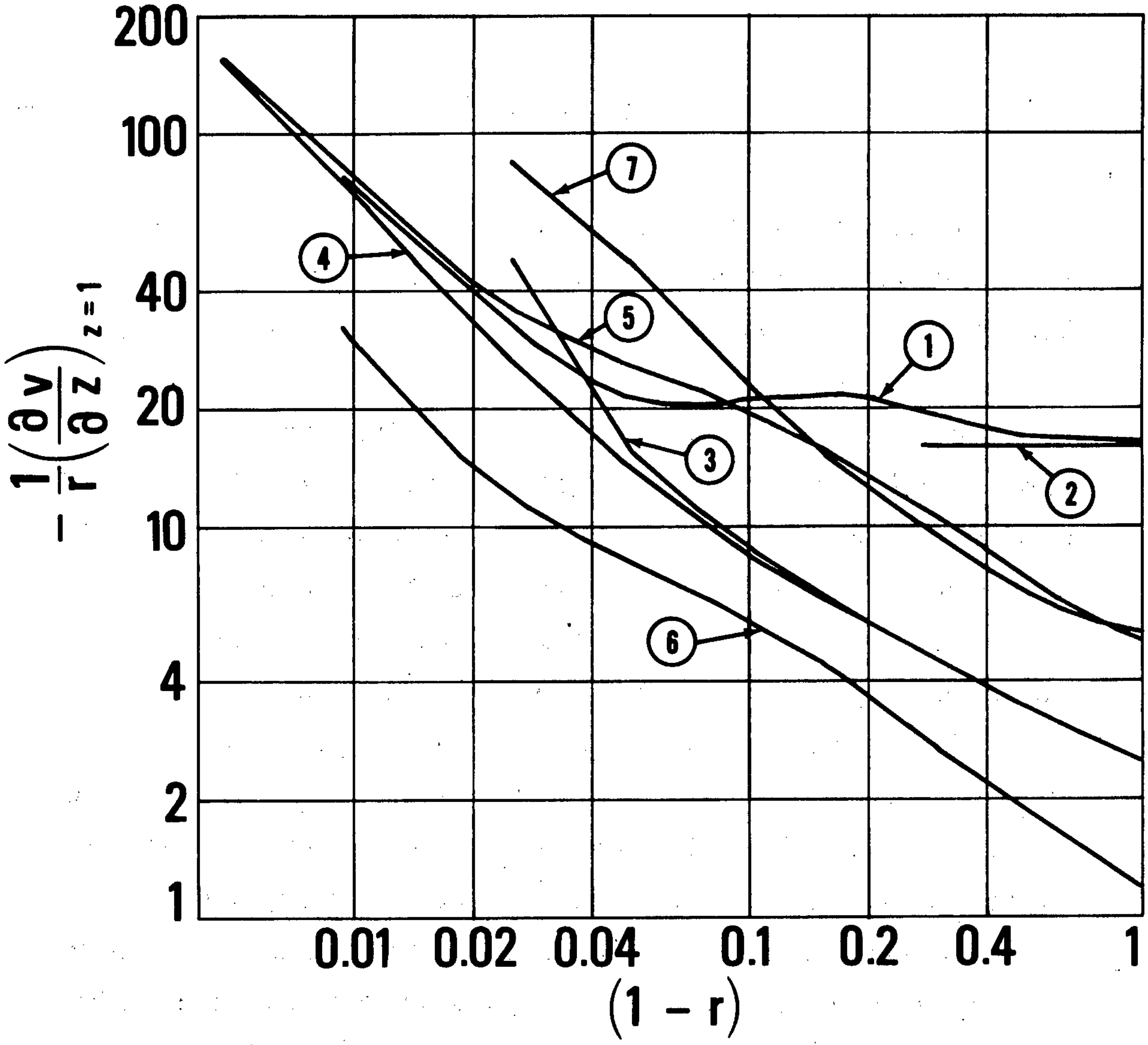

(1) $Ro = 10^{-5}$ $Ek = 10^{-3}$, $\delta = 1$

(2) EKMAN SOLUTION

(3) $Ro = 1$, $Ek = 0.01$, $\delta = 1$, $a = 0$, $b = 0.1$

(4) $Ro = 1$, $Ek = 0.01$, $\delta = 1$, $a = 0.26$, $b = 0.13$

(5) $Ro = 1$, $Ek = 10^{-3}$, $\delta = 1$

(6) $Ro = 1$, $Ek = 0.01$, $\delta = 1/3$

(7) $Ro = 1$, $Ek = 0.01$, $\delta = 3$

Figure 14 - $-\frac{1}{r}(\partial v/\partial z)_{z=1}$ as a Function of 1-r for Various Ro, Ek, and δ

$$f = \frac{2m}{\sqrt{\ell^2 + m^2}} , \qquad (30)$$

where ℓ and m are the eigenvalues for the r- and z-components, respectively. The waves connected with these modes are called "inertial waves"[9]. The zero mode, which is time-independent, represents the geostrophic motion.

Modifications of the inviscid flows occur in the Ekman and Stewartson layers in order to satisfy the boundary condition of no-slip. In Figure 15 a sequence of ψ - and v-patterns for $Ro = 10^{-5}$, $Ek = 0.001$, $\delta = 1$ over the transient period is presented. A more detailed time history for the same case is recorded in Figure 16, where $-(\zeta/r)_{r=0}$ at the cover and at the bottom is plotted against time. After the sudden change of the cover's angular speed, a boundary layer on the cover develops whose $-(\zeta/r)_{r=0}$ -value reaches a peak at t = 1.5. This time agrees with the spin-up theory which estimates $t \approx 1$ for the initial phase[9]. Afterwards, inertial oscillations are visible. They appear in the streamline patterns in the form of temporal oscillations and produce cell-type motions in the center of the tank (Figure 15, t = 3.98, 9.98). With increasing time the inertial oscillations are damped, the local cell vanishes, anf the flow reaches a steady state. Both curves in Figure 16 approach asymptotically the value $\frac{1}{2} Ek^{-1/2} = 15.811$ of the Ekman-layer solution.

With increasing Ekman number the influence of viscosity is felt in the interior. In Figure 17 the function $-(\zeta/r)_{r=0}$ at the cover and at the bottom is plotted against time for $Ro = 10^{-5}$, $Ek = 0.01$, $\delta = 1$. Inertial oscillations have almost vanished. In

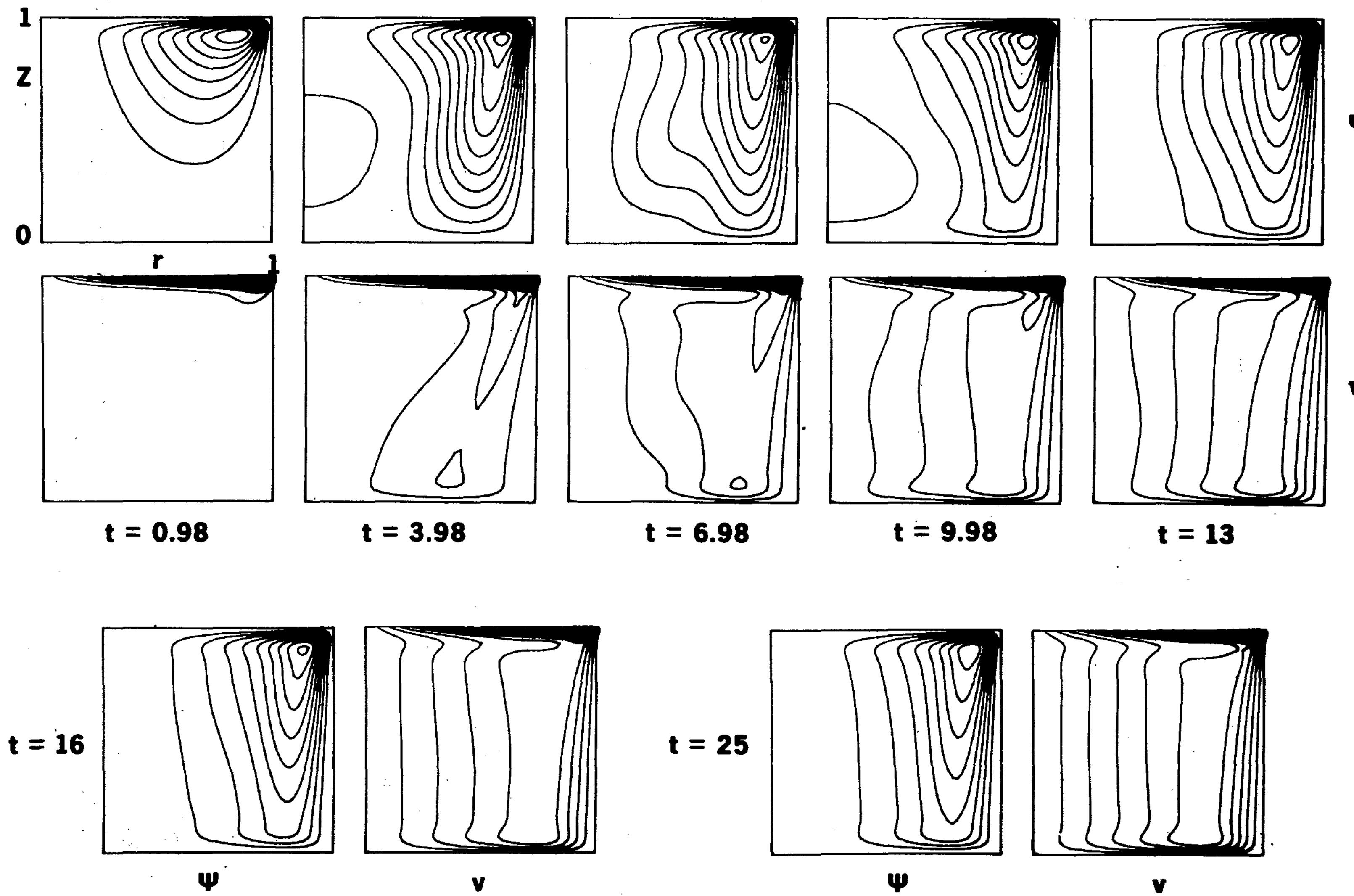

Figure 15 - Lines of Constant ψ and v for Ro = 10^{-5}, Ek = 0.001, δ = 1 at Various t. The almost Steady State at t_{FINAL} = 103 is included in Figure 2

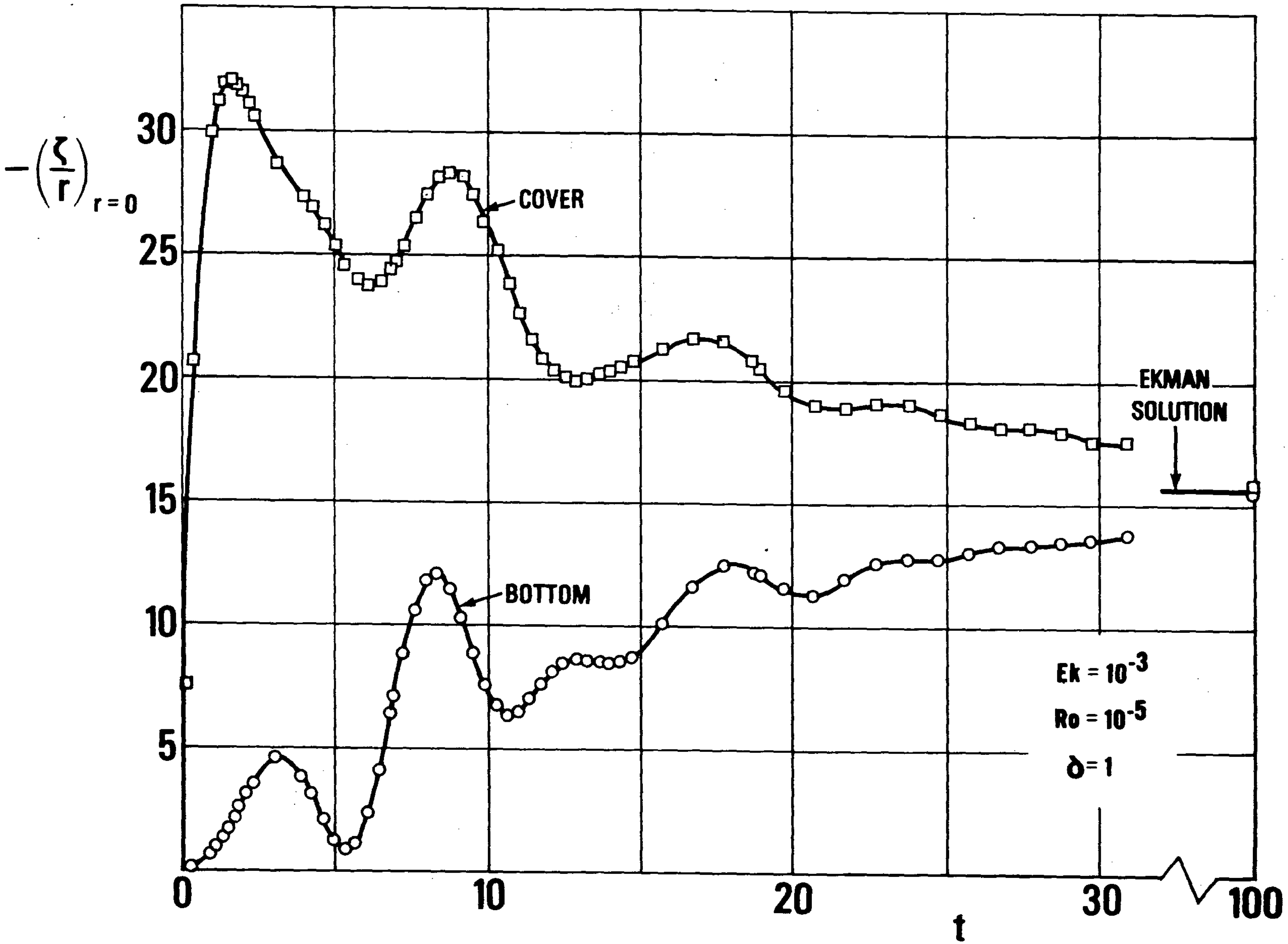

Figure 16 - $-(\zeta/r)_{r=0}$ at Bottom and Cover as a Function of t for Ro = 10^{-5}, Ek = 0.001, δ = 1

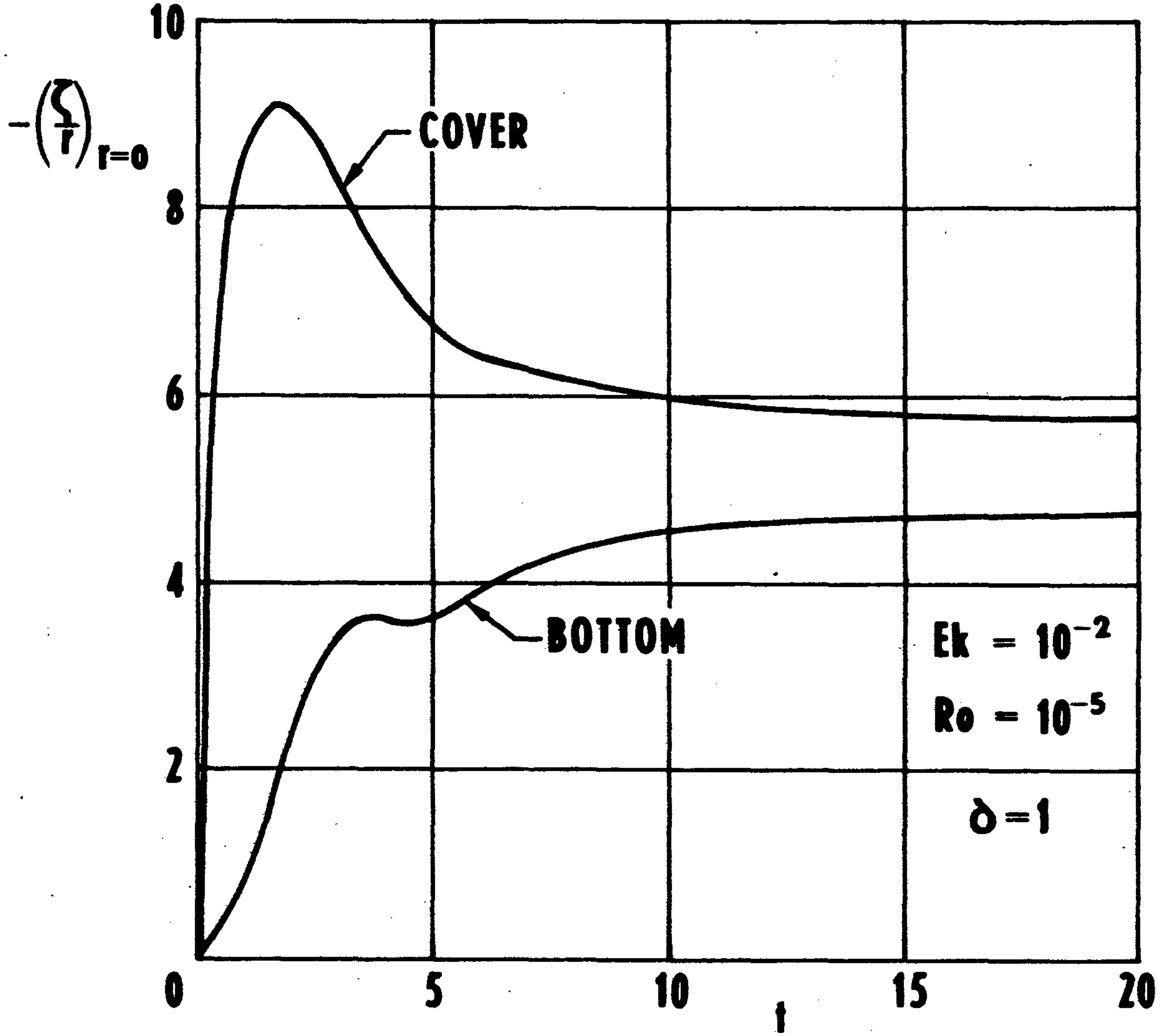

Figure 17 - $-(\zeta/r)_{r=0}$ at Bottom and Cover as a Function of t for Ro = 10^{-5}, Ek = 0.01, δ = 1

Figure 18 the flow behavior away from the boundary layers is displayed. The function $-(v/r)_{r=0}$ at $z = \frac{1}{2}$ is plotted against time for both Ek = 0.001 and Ek = 0.01 (Ro = 10^{-5}, δ = 1). Inertial oscillations are observed only for the flow with the smaller Ekman number. No single mode can be identified. This indicates the existence of nonzero eigenvalues ℓ in Equation (30).

As long as the Ekman number is sufficiently small, that is, Ek $<<$ 0.01, inertial oscillations also occur if nonlinear effects are present. For Ro = 1, Ek = 0.001, δ = 1 a time sequence of ψ- and v-patterns is shown in Figure 19. Again, a cell is visible in the center of the tank as in the linear case Ro = 10^{-5}, Ek = 0.001. A new phenomenon in Figure 19 is the appearance of a local region of positive v. Pao[3] computed the case Ro = 1, Ek = 0.001 up to t = 4.2. His streamlines agree well with ours, but his picture does not show the local cell at t = 4.2.

For Ro = 1, Ek = 0.001, δ = 1 a computer-generated movie has been made which shows the transient stage for ψ and v. The movie clearly reveals the time oscillations which cannot easily be detected in Figure 19.

Higher order modes are observed for decreasing Ekman number. In Figures 20 and 21 the ψ- and v-patterns are displayed for the transient period of the case Ro = 1, Ek = 0.0002, δ = 1. At t = 4.50 and 11.25 two cells at the centerline are visible. The whole sequence shows three distinct time periods when local cells are present. It may be mentioned that Pao[3] computed this case up to t = 3.0. His strong undulations of the streamlines near the singular point are not verified by our calculations.

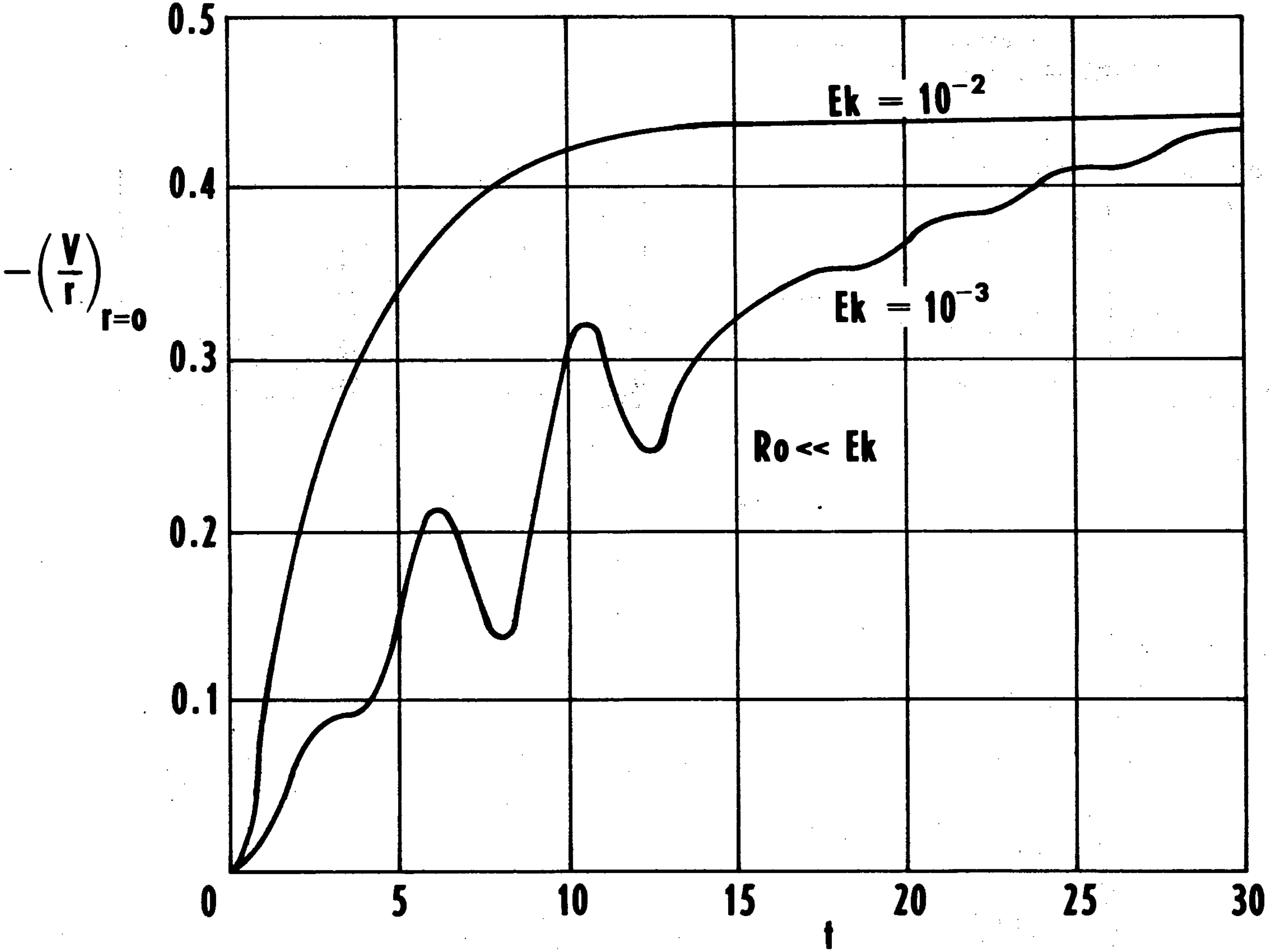

Figure 18 - $-(v/r)_{r=0}$ at $z = 1/2$ as a Function of t for $Ro = 10^{-5}$, $\delta = 1$, $Ek = 0.001$ and 0.01

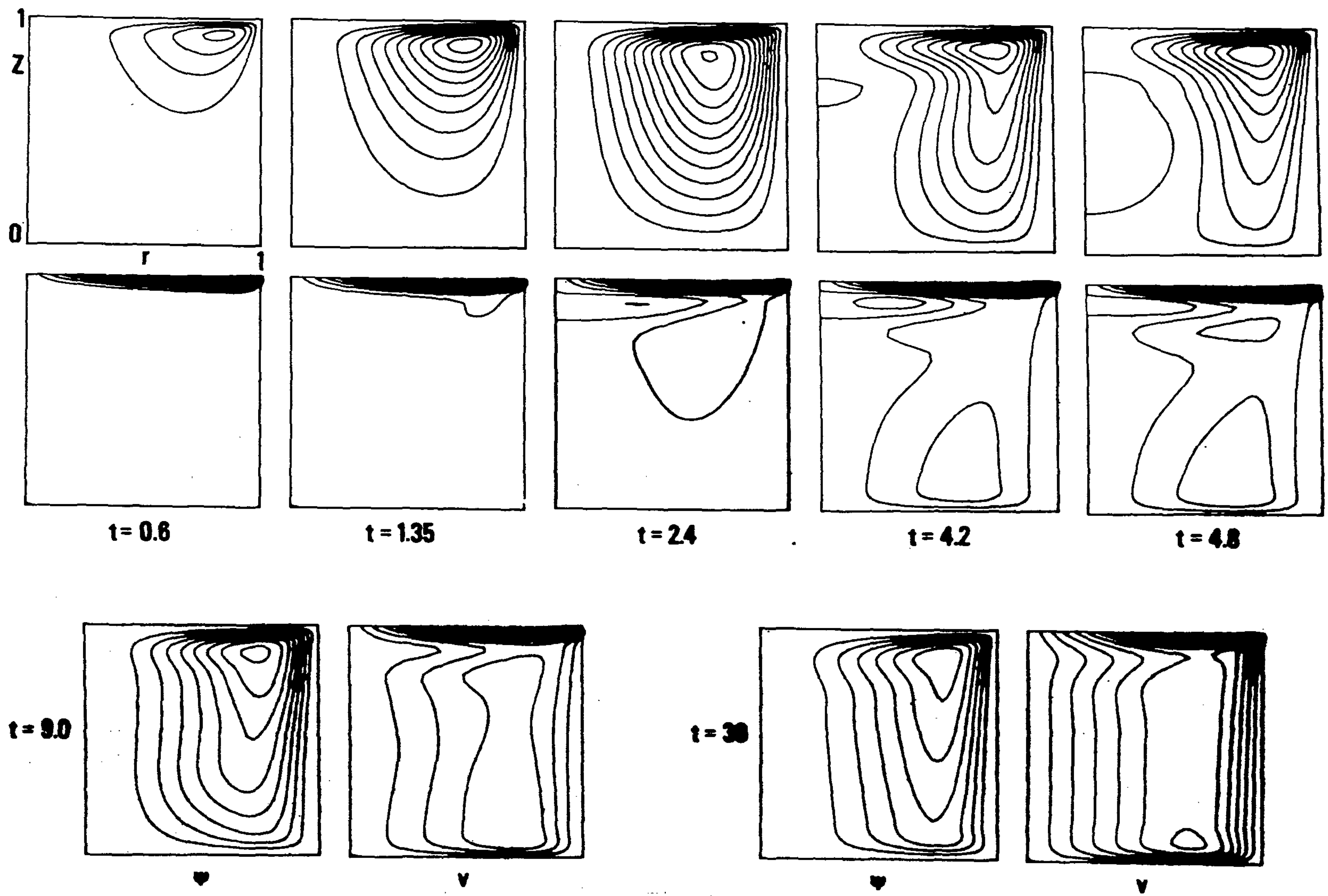

Figure 19 - Lines of Constant ψ and v for Ro = 1, Ek = 0.001, δ = 1 at Various t. The almost Steady State at t_{FINAL} = 102 is Included in Figure 7

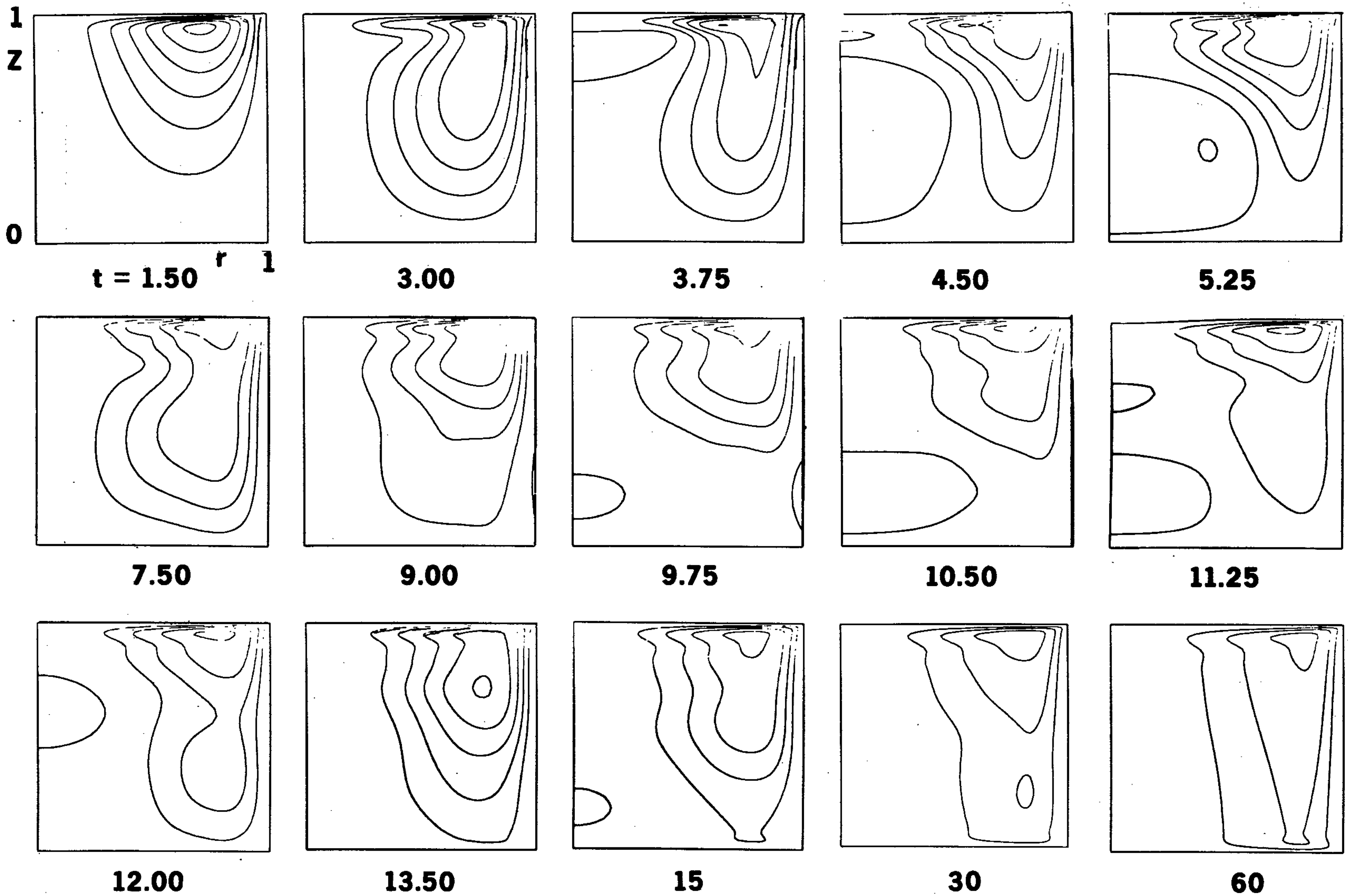

Figure 20 - Lines of Constant ψ for Ro = 1, Ek = 0.0002 δ = 1 at Various t. The almost Steady State at t_{FINAL} = 245 is Included in Figure 8

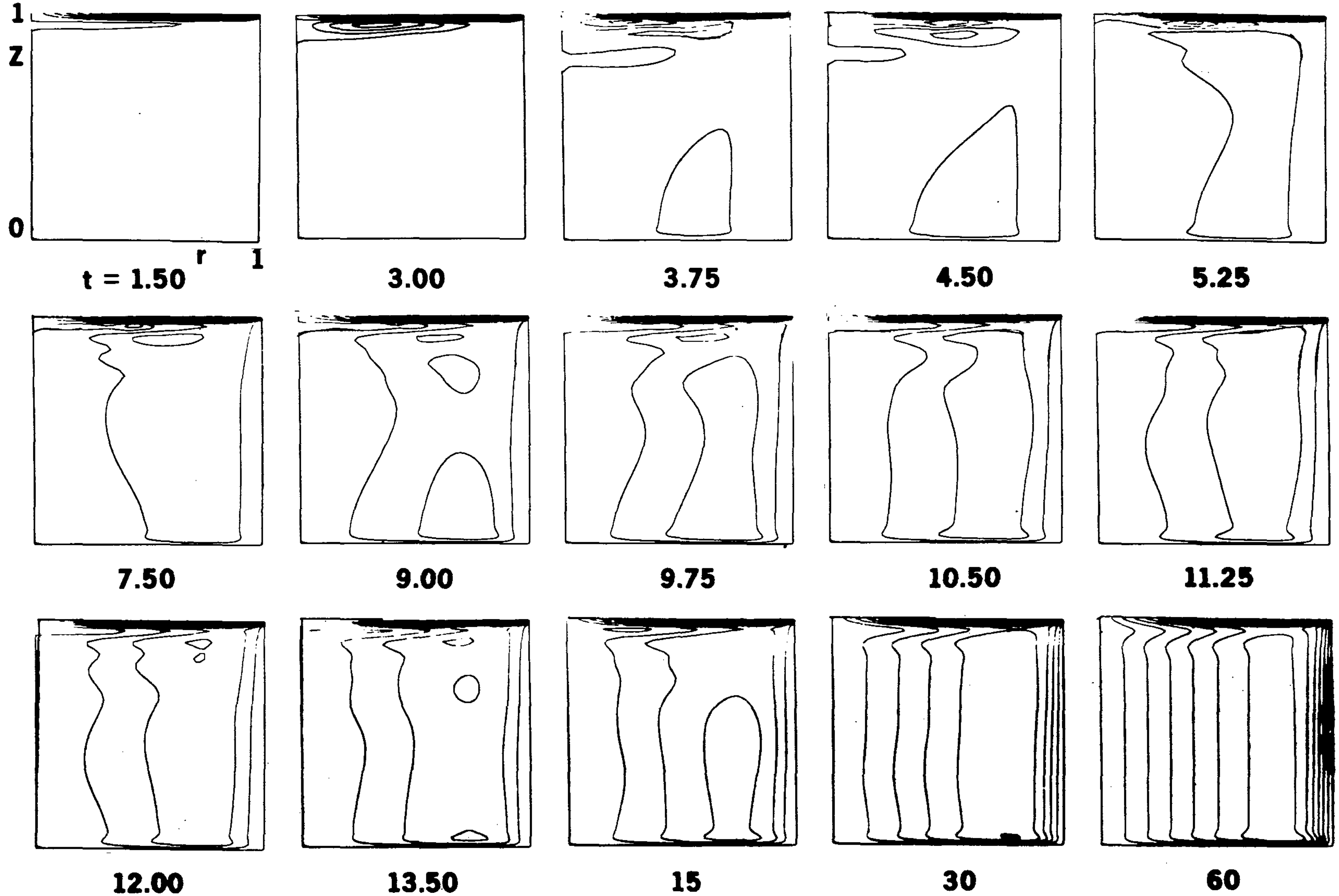

Figure 21 - Lines of Constant v for Ro = 1, Ek = 0.0002, δ = 1 at Various t. The almost Steady State at t_{FINAL} = 245 is Included in Figure 8

Finally, a time sequence of constant ψ, ζ, and v curves is presented for Ro = 10, Ek = 0.01, $\delta = 1$ in Figure 22. At this high Rossby number the oscillations are shifted toward the sidewall.

5. CONCLUSIONS

Simple geometrical tank configurations with simple initial and boundary conditions for the fluid inside can generate complicated flow circulations. In the transient period inertial waves are visible in the form of oscillating streamlines and cell motions without preferred mode. In the steady-state case monotonic and undulating streamline patterns are distinguished.

The numerical analysis which was developed for nonrotating motion also works well for rotating flows with hyperbolic features. The numerical calculations have been restricted to flows with Ek $\geq$ 0.0002 (for Ro = 1) since the assumption of axisymmetry does not seem to be justified for smaller Ek.

The linear theory developed in literature on the basis of perturbation methods is restricted for the case Ro $\ll$ Ek $\ll$ 1 to Ek $\leq 10^{-3}$ (for $\delta = 1$) and for slow motion according to Reference 3 to Ek $>$ 0.125 (for Ro = 1, $\delta = 1$).

As $\delta \rightarrow 0$ the computed values approach the similarity solutions for two infinite disks.

The infinitely thin gap between side wall and cover causes a flow singularity which, although local and very weak, results always in an infinite torque. For practical applications a nonvanishing gap width must be considered. The strength of the torque appears to depend crucially on this width (see also Reference 13).

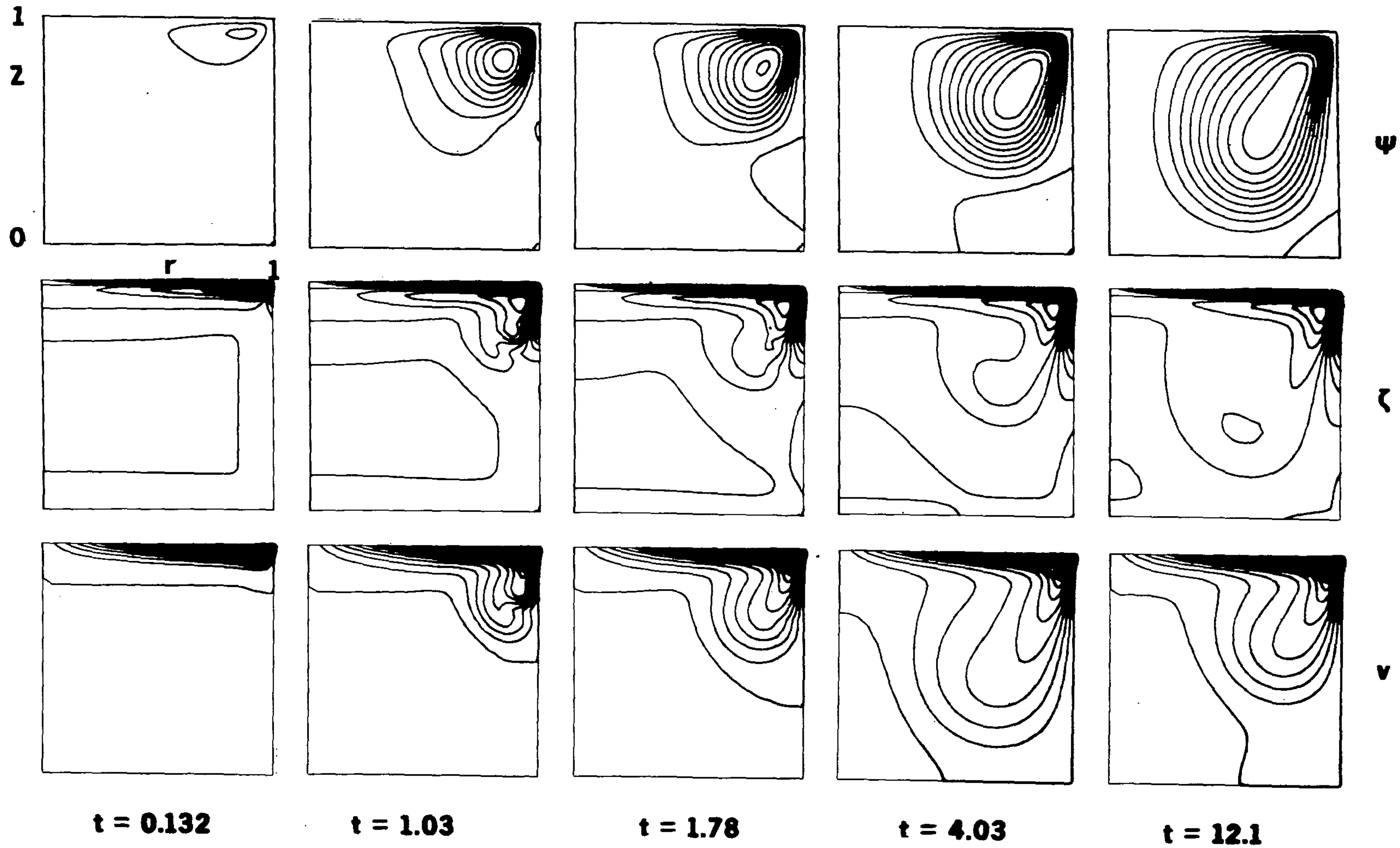

Figure 22 - Lines of Constant ψ, ζ, and v for Ro = 10, Ek = 0.01, δ = 1 at Various t. The almost Steady State at t_{FINAL} = 50 is Included in Figure 8

ACKNOWLEDGMENT

The authors would like to thank Mr. J.K. Reingruber for plotting the pathline in Figure 13 with his newly developed program VIEWPLOT.

REFERENCES

1. Dorfman, L.A. and Romanenko, Y.B., Izv. AN SSSR, Mechanika Zhidkosti i Gaza, 1, 63 (1966).

2. Pao, H.P., Dept. Space Science and Applied Physics, Catholic University of America, Report No. 70-005, July 1970.

3. Pao, H.P., Journ. Appl. Mech. 37, 480 (1970).

4. Farris, G.J. et al., Union Carbide Corporation, Nuclear Division, Oak Ridge, Rep. No. CTC-7, March 1969.

5. Krause, E., DFVLR-Kolloquium 1970, Porz-Wahn, Institut für Angewandte Gasdynamik, 93.

6. Rasmussen, H., Zeitschrift für Angewandte Mathematik und Physik, 21, 611 (1970).

7. Briley, W.R. and Walls, H.A., Proceedings Second International Conference on Numerical Methods in Fluid Dynamics, Sept. 15-19, 1970, University of California, Berkeley.

8. Schlichting, H., Boundary-Layer Theory, Verlag G. Braun, Karlsruhe, Sixth Ed., 1968.

9. Greenspan, H. P., The Theory of Rotating Fluids, Cambridge University Press, 1968.

10. Pearson, C. E., J. Fluid Mech., 21, 623 (1965).

11. Euteneuer, G. A., et al., Acta Mechanica, 5, 237 (1968).

12. Lugt, H. J. and Haussling, H. J., Proceedings Second International Conference on Numerical Methods in Fluid Dynamics, Sept. 15-19, 1970, University of California, Berkeley.

13. Schmieden, C., Zeitschrift für Angewandte Mathematik und Mechanik, 8, 460 (1928).

14. Hort, W., Zeitschr. techn. Physik, 1, 213 (1920).

15. Lance, G. N. and Rogers, M. H., Proc. Roy. Soc. A., 266, 109 (1962).

16. Barcilon, V., Phys. Fluids, 13, 537 (1970).

17. Schwiderski, E. W., and Lugt, H. J., Ingenieur-Archiv, 34, 198 (1965).

INITIAL DISTRIBUTION

Copies		Copies	
7	CHONR 1 Dr. P. King (102) 1 Mr. M. Cooper (430B) 1 Dr. L. D. Bram (432) 1 Dr. R. D. Ryan (434) 1 Dr. B. J. Macdonald (436) 1 Mr. R. D. Cooper (438)	1	CO, U.S. Naval ROTC & Administrative Unit, MIT
1	DNL	1	Naval War College
1	NRL, Tech Lib	1	NAVSHIPYD BREM
4	NAVSHIPSYSCOM 1 SHIPS 031 1 SHIPS 0311 2 SHIPS 2052	1	NAVSHIPYD BSN
1	NELC, Tech Lib	1	NAVSHIPYD CHASN
1	NURDC, Tech Lib	1	NAVSHIPYD HUNTERS PT
1	NWC, Tech Lib	1	NAVSHIPYD LBEACH
1	NOL, Tech Lib	1	NAVSHIPYD MARE ISLAND
7	NWL 1 Mr. B. Smith (D) 1 Dr. C. J. Cohen (K) 1 Dr. A. V. Hershey (KXH) 1 Dr. E. W. Schwiderski (KXS) 1 Dr. P. Ugincius (KXU) 1 Dr. B. Zondek (KXZ) 1 Tech Lib	1	NAVSHIPYD NORVA
2	SUPT, USNA 1 Dept of Math 1 Tech Lib	1	NAVSHIPYD PEARL
4	SUPT, PGSCHOL, Monterey 1 Lib, Tech Rept Sec 1 Math Dept 1 Dr. T. H. Gawin 1 Prof. T. Sarpkaya	1	NAVSHIPYD PHILA
		1	NAVSHIPYD PTSMH
		12	DDC
		2	U.S. Army Math Res Ctr, Univ of Wisconsin, Madison 1 Dr. D. Greenspan 1 Tech Lib
		1	U. S. Army Res Off, Durham, N.C. 27706 CRD-AA-IPL Box CM
		1	NASA, Wash D. C., Tech Lib.
		1	NASA, Marshal Space Flight Ctr. Huntsville, Ala 35809, Tech Lib
		1	NASA, Lewis Res Ctr, Cleveland, Ohio 44121

Copies

3 NASA, Ames Res Ctr, Moffet Field, Calif. 94305
1 Dr. W. J. McCroskey
1 Dr. E. D. Martin
1 Tech Lib

1 NASA, Langley Field, Tech Lib

4 Los Alamos Sci Lab, Los Alamos, New Mexico 87544
1 Dr. F. H. Harlow
1 Dr. C. W. Hirt
1 Dr. B. J. Daly
1 Tech Lib

2 Brookhaven Nat Lab, Upton, Long Island, N. Y.
1 Dr. P. Michael
1 Tech Lib

3 National Bureau of Standards
1 Dr. H. Oser
1 Dr. W. Sadowski
1 Tech Lib

2 Nat Sci Foundation, 1520 H St., N.W., Wash D.C. 20550
1 Eng Sci Div
1 Math Sci Div

4 Princeton Univ
1 Prof. S. I. Cheng
1 Dr. J. Smagorinsky
1 Dr. K. Bryan
1 Aerospace and Mech Eng Lib
1 Prof. M. Kruskal

2 Harvard Univ
1 Prof. G. Birkhoff
1 Prof. F. G. Carrier

4 M.I.T., Cambridge, Mass
1 Prof. J. G. Charney
1 Prof. C. C. Lin
1 Prof. S. A. Orszag
1 Prof. H. P. Greenspan

Copies

3 Univ of Maryland, College Pk, Md.
1 Prof. A. J. Faller
1 Prof. A. Plotkin
1 Prof. D. Sallet

1 USAEC, Tech Lib

1 Oak Ridge Nat Lab., Tech LIb

3 Courant Inst of Math Sci, N.Y. Univ, New York, N. Y.
1 Prof. H. B. Keller
1 Dr. A. J. Chorin
1 Dr. Burstein

2 Stanford Univ
1 Prof. A. Acrivos
1 Prof. M. D. Van Dyke

3 Brown Univ, Prov, R. I.
1 Prof. W. Prager
1 Prof. J. Kestin
1 Prof. M. Sibulkin

2 Poly Inst of Brooklyn
1 Prof. G. Moretti
1 Prof. R. C. Ackerberg

3 Nat'l Cntr for Atmospheric Research, Boulder, Colorado 80301
1 Dr. D. K. Lilly
1 Dr. A. Kasahara
1 Dr. J. W. Deardorff

1 Prof. J. S. Allen, Penn St Univ, Dept of Aerospace Eng, Univ Pk, Pa 16802

1 Dr. J. E. Fromm
Dept 977, Bldg 025, Res Div, IBM Corp, Monterey and Cottle Road, San Jose, Calif 95114

1 Dr. C. W. van Atta
Univ of Calif, La Jolla, Calif 92037

Copies

1 Dr. E. R. van Driest
North American Rockwell Corp.
350 So. Magnolia Ave, Long
Beach, Calif. 90802

1 Prof. W. W. Wilmarth
Univ of Mich, 1077 East Eng
Bldg, Ann Arbor, Mich 48104

1 Univ of Notre Dame
1 Prof. A. A. Szewczyk

2 West Virginia Univ, Morgantown,
West Virginia
1 Prof. J. B. Fanucci
1 Prof. W. Squire

1 Dr. D. Thoman
C23 E. Mishawaha Ave.,
Mishawaha, Indiana

1 Prof. Z. Lavan
Illinois Inst of Tech,
Chicago, Illinois 60616

1 Prof. K. E. Torrance
Cornell Univ, Ithaca, N.Y.

1 Prof. M.Z.v. Krzywoblocki
Mich St Univ, East Lansing,
Mich

1 Dr. W. E. Langlois
IBM Res Lab, San Jose, Calif

1 Prof. J. Happel
Dept Chemical Eng, New York
Univ, New York

1 Hq, American Society of Naval
Engineers, 1012 14th St, N. W.
Washington, D.C. 20005

Copies

1 Dr. M. V. Morkovin
Dept Mechanical & Aerospace
Eng, Ill Institute of Technology
Chicago, Illinois 60616

1 Dr. Vivian O'Brien
The Johns Hopkins Univ
Applied Physics Lab, 8621
Georgia Ave, Silver Spring,
Md, 20910

1 Prof. James C. Wu
School of Aerospace Eng,
Georgia Institute of Tech,
Atlanta, Georgia 30332

1 Prof. Edmund V. Laitone
Div of Aeronautical Sciences
Univ of California, Berkeley
Calif, 94720

1 Prof. Raymond E. Goodson
Purdue University, Automatic
Control Center, School of
Mech Eng, Lafayette, Indiana
47907

1 Mr. Stanley K. Jordan
The Analytic Sciences Corp.
6 Jacob Way, Reading,
Massachusetts 01867

CENTER DISTRIBUTION

Copies	
1	01
1	15
1	154
1	1541
1	16
1	18
1	1802.2
100	1802.3
1	1805
1	184
5	1843
2	1892

DOCUMENT CONTROL DATA - R & D

(Security classification of title, body of abstract and indexing annotation must be entered when the overall report is classified)

1. ORIGINATING ACTIVITY *(Corporate author)* Naval Ship R&D Center Bethesda, Maryland 20034	2a. REPORT SECURITY CLASSIFICATION UNCLASSIFIED 2b. GROUP

3. REPORT TITLE

Laminar Flow Circulation in a Rotating Tank with a Spinning Cover

4. DESCRIPTIVE NOTES *(Type of report and inclusive dates)*

5. AUTHOR(S) *(First name, middle initial, last name)*

Hans J. Lugt
Henry J. Haussling
Samuel Ohring

6. REPORT DATE	7a. TOTAL NO. OF PAGES	7b. NO. OF REFS
February 1972	53	8

8a. CONTRACT OR GRANT NO.	9a. ORIGINATOR'S REPORT NUMBER(S) 3797
b. PROJECT NO. SR 003-03-01 c. d.	9b. OTHER REPORT NO(S) *(Any other numbers that may be assigned this report)*

10. DISTRIBUTION STATEMENT

Approved for Public Release; Distribution Unlimited

11. SUPPLEMENTARY NOTES	12. SPONSORING MILITARY ACTIVITY
	Naval Ship Systems Command

13. ABSTRACT

A study has been made of axisymmetric incompressible fluid flows in a rotating tank when the angular speed of the cover changes abruptly. From the initial solid-body rotation a meridional and an azimuthal circulation relative to the moving tank develop. This problem is solved numerically by means of a stream function-vorticity formulation for the meridional flow. Local fine grids are used in the Ekman and Stewartson layers. No finite gap between tank and cover is considered. The singular behavior at this point is investigated. The parameters considered are the Rossby number, the Ekman number, and the ratio of height to radius of the tank. Temporal and spatial oscillations of the laminar flow field as well as the occurrence of cell flows are discussed.

14. KEY WORDS	LINK A		LINK B		LINK C	
	ROLE	WT	ROLE	WT	ROLE	WT
Rotating Tank Flow Circulation Ekman Layer Stewartson Layer						